bioRxiv preprint doi: https://doi.org/10.1101/372946; this version posted July 20, 2018. The copyright holder for this preprint (which was not certified by peer review) is the author/funder, who has granted bioRxiv a license to display the preprint in perpetuity. It is made available under aCC-BY 4.0 International license.

Glycolytic flux in *Saccharomyces cerevisiae* is dependent on RNA polymerase III and its negative regulator Maf1

Róża Szatkowska[1], Manuel Garcia-Albornoz[2], Katarzyna Roszkowska[1], Stephen Holman[3], Simon Hubbard[2], Robert Beynon[3], Malgorzata Adamczyk *[1]

[1]Chair of Drug and Cosmetics Biotechnology, Faculty of Chemistry, Warsaw University of Technology, Poland

[2]Division of Evolution & Genomic Sciences , School of Biological Sciences, Faculty of Biology, Medicine and Health, Manchester Academic Health Science Centre, University of Manchester, UK

[3]Centre for Proteome Research, Institute of Integrative Biology, University of Liverpool, Liverpool, UK

Corresponding author: madamczyk@ch.pw.edu.pl

bioRxiv preprint doi: https://doi.org/10.1101/372946; this version posted July 20, 2018. The copyright holder for this preprint (which was not certified by peer review) is the author/funder, who has granted bioRxiv a license to display the preprint in perpetuity. It is made available under aCC-BY 4.0 International license.

Abstract

Protein biosynthesis is energetically costly, is tightly regulated and is coupled to stress conditions including glucose deprivation. RNA polymerase III (RNAP III) driven transcription of tDNA genes for production of tRNAs is a key element in efficient protein biosynthesis. Here we present an analysis of the effects of altered RNAP III activity on the *Saccharomyces cerevisiae* proteome and metabolism under glucose rich conditions. We show for the first time that RNAP III is tightly coupled to the glycolytic system at the molecular systems level. Decreased RNAP III activity or the absence of the RNAP III negative regulator, Maf1 elicit broad changes in the abundance profiles of enzymes engaged in fundamental metabolism in *S. cerevisiae*. In a mutant compromised in RNAP III activity there is a repartitioning towards amino acids synthesis *de novo* at the expense of glycolytic throughput. Conversely, cells lacking Maf1 protein have greater potential for glycolytic flux.

bioRxiv preprint doi: https://doi.org/10.1101/372946; this version posted July 20, 2018. The copyright holder for this preprint (which was not certified by peer review) is the author/funder, who has granted bioRxiv a license to display the preprint in perpetuity. It is made available under aCC-BY 4.0 International license.

Introduction

Regulation of glycolytic flux is a long standing, but still highly relevant, issue in biology and pathobiology. Glycolytic performance is connected to enzymes abundance, cell fermentative activity and proliferation, all hallmarks of the "Warburg effect". Both *Saccharomyces cerevisiae* and mammalian cells can sense glycolytic state/flux intracellularly, a dominant signal over that of external nutritional status [1–4]. In *Saccharomyces cerevisiae* under favorable growth conditions, high glycolytic activity elicits rapid cell growth, due to robust synthesis of proteins and biomass expansion [5–7]. Nutrient limited growth, on the other hand, is associated with a down regulation of transcription and protein synthesis to reduce demands on the ribosomal machinery and an appropriate supply of amino acids and tRNAs.

As key players in protein synthesis, transfer RNAs are synthesized by RNA Polymerase III (RNAP III), which is also responsible for the transcription of other specific products such as ribosomal 5S rRNA and spliceosomal U6 snRNA. RNAP III activity is regulated by extracellular glucose levels [8,9]. The only known direct regulatory factor of RNAP III in *S. cerevisiae* is the protein Maf1, a mediator of a range of stress signals [10–13] conserved from yeast to human [14]. Yeast Maf1 inhibits RNAP III activity reversibly under carbon source starvation and oxidative stress, reducing tRNA transcript levels [15]. Although the *MAF1* gene is not essential for yeast viability, *maf1Δ* cells are unable to repress RNAP III [15–18].

Under favorable growth conditions, Maf1 is an interaction partner of several cytoplasmic proteins playing different biological functions (Fig 1 A and B), but its function in the cytoplasm is unknown. Maf1 is a target of several kinases and phosphorylation patterns may dictate cellular localization [15,19–25] (Fig 1 B). Although *MAF1* deletion is not lethal under optimal growth conditions, deletion mutants display high tRNA transcription with diminished growth on non-fermenting carbon sources at 30°C; it becomes lethal, however, at elevated temperatures. The low growth rate results from a decrease in steady state mRNA levels of *FBP1* and *PCK1* genes encoding the key gluconeogenesis enzymes fructose 1,6 bisphosphatase (Fbp1) and phosphoenolpyruvate carboxykinase (Pck1) [10,26]. Intriguingly, this *maf1Δ* growth defect on non-fermentable carbon sources is suppressed by point mutation (*rpc128-1007)* in the second largest RNAP III subunit *RET1*/C128 [13]. tRNA transcription levels in this *rpc128-1007* mutant are very low, which suggests that the

bioRxiv preprint doi: https://doi.org/10.1101/372946; this version posted July 20, 2018. The copyright holder for this preprint (which was not certified by peer review) is the author/funder, who has granted bioRxiv a license to display the preprint in perpetuity. It is made available under aCC-BY 4.0 International license.

68 temperature-sensitive lethality of *maf1Δ* can be rescued by attendant reduction of RNAP III activity, or a critical
69 process affected by this transcription. The *maf1Δ* and *rpc128-1007* strains have different phenotypes, not only
70 in growth on non-fermentable carbon sources, but also in preference towards glucose utilization, in excess
71 glucose [13,27]. Transcription of the high affinity glucose transporter genes *HXT6, HXT7* is decreased in *maf1Δ*,
72 but increased over WT in the *maf1Δ* second-site suppressor *rpc128-1007* [27], suggesting differences in glucose
73 utilization.
74
75 We wished to explore the potential for a feedback loop between control of glycolytic flux and RNAP III in yeast
76 cells by label free proteomics, which revealed changes in abundance of a large group of proteins in *maf1Δ* and
77 *rpc128-1007* strains, supported with targeted analysis of specific metabolites. We provide novel molecular data
78 which is able to explain the severe reduction in growth rate caused by RNAP III mutation *rpc128-1007* through
79 cellular processes that facilitate efficient glucose metabolism in the *MAF1* deletion strain on glucose. Changes
80 in protein profiles impact several metabolic pathways, suggesting differences in cellular metabolic
81 homoeostasis in the mutant strains and providing an alternative explanation for *maf1Δ* lethality on non-
82 fermentable carbon sources. Finally, using yeast as a model organism, which is often used for studies of the
83 "Warburg effect", we established direct metabolic relationship between the capacity of the glycolytic pathway
84 and transcription of non-coding genes, which can explain why several cancerous cell lines exhibit higher RNAP
85 III activity, creating a new perspective on glucose flux modification *via* manipulation of the RNAP III holoenzyme
86 as an novel therapeutic strategy.
87
88

bioRxiv preprint doi: https://doi.org/10.1101/372946; this version posted July 20, 2018. The copyright holder for this preprint (which was not certified by peer review) is the author/funder, who has granted bioRxiv a license to display the preprint in perpetuity. It is made available under aCC-BY 4.0 International license.

Materials and Methods

Yeast strains and media.

The following strains were used: wild-type MB159-4D [28] with unchanged RNAP III activity, the MA159-4D *maf1::URA3* [27] *MAF1*-deficient mutant with elevated RNAP III activity and MJ15-9C mutant [13] with a single point mutation in the *RET1/C128* RNAP III subunit with reduced polymerase activity. Yeast strains were cultured in rich medium (YP; 1% yeast extract, 1% peptone) supplemented with either 2% glucose (YPD) or 2% glycerol (YPGly) as a carbon source. Overnight cell cultures were grown in YPD medium. Cells were harvested by centrifugation (2000 rpm, RT) and washed twice with fresh, sterile YPD or YPGly medium. Yeast cells were diluted to $A_{600} \approx 0.1$ and grown in YPD or YPGly until exponential phase ($A_{600} \approx 1.0$). All yeast cultures were incubated in 30°C with agitation 250 rpm. *GCN4-3HA* DNA construct for chromosomal C-terminus fusion was prepared as described previously [27,29]. Hexokinase isoforms (*HXK1, HXK2, GLK1*) single and double gene deletions were created by transforming haploid yeast strains with appropriate PCR fragments. For *HXK1* deletion amplification of *His3MX6* cassette on *pFA6-VC155-His3MX6* plasmid DNA was done. DNA constructs for obtaining *HXK2* and *GLK1* deficient strains were amplified on gDNA of BY4741 *glk1Δ* and BY4741 *hxk2Δ* (Euroscarf). High-efficiency yeast transformation using LiAc/SS carrier DNA/PEG method was used according to Gietz [30]. All yeast strains are listed in Table 1.

Table 1. Yeast strains used in the study.

Strain	Genotype	Reference/ Source
MB159-4D	MATa SUP11 ura3 leu2-3, 112 ade2-1 lys2-1 trp	[10]
MA159-4D *maf1Δ*	MATa SUP11 ura3 leu2-3, 112 ade2-1 lys2-1 trp *maf1::URA3*	[27]
MB159-4D *maf1Δ*	MATa SUP11 ura3 leu2-3, 112 ade2-1 lys2-1 trp *maf1::kanMX6*	[28]
MJ15-9C	MATa *rpc128-1007* SUP11 ura3 leu2-3, 112 ade2-1 lys2-1 trp	[13]

bioRxiv preprint doi: https://doi.org/10.1101/372946; this version posted July 20, 2018. The copyright holder for this preprint (which was not certified by peer review) is the author/funder, who has granted bioRxiv a license to display the preprint in perpetuity. It is made available under aCC-BY 4.0 International license.

RS159-4D Gcn4-3HA	MATa SUP11 ura3 leu2-3, 112 ade2-1 lys2-1 trp *Gcn4-3HA-kanMX6*	This study
RS15-9C Gcn4-3HA	MATa *rpc128-1007* SUP11 ura3 leu2-3, 112 ade2-1 lys2-1 trp *Gcn4-3HA-kanMX6*	This study
RS159-4D *maf1Δ* Gcn4-3HA	MATa SUP11 ura3 leu2-3, 112 ade2-1 lys2-1 trp *maf1::URA3 Gcn4-3HA-kanMX6*	This study
KR159-4D *hxk1Δ*	MATa SUP11 ura3 leu2-3, 112 ade2-1 lys2-1 trp *hxk1::HIS3MX6*	This study
KR159-4D *maf1Δ hxk1Δ*	MATa SUP11 ura3 leu2-3, 112 ade2-1 lys2-1 trp *maf1::URA3 hxk1::HIS3MX6*	This study
KR15-9C *hxk1Δ*	MATa *rpc128-1007* SUP11 ura3 leu2-3, 112 ade2-1 lys2-1 trp *hxk1::HIS3MX6*	This study
KR159-4D *hxk1Δ hxk2Δ*	MATa SUP11 ura3 leu2-3, 112 ade2-1 lys2-1 trp *hxk1::HIS3MX6 hxk2::kanMX4*	This study
KR159-4D *maf1Δ hxk1Δ hxk2Δ*	MATa SUP11 ura3 leu2-3, 112 ade2-1 lys2-1 trp *maf1::URA3 hxk1::HIS3MX6 hxk2::kanMX4*	This study
KR15-9C *hxk1Δ hxk2Δ*	MATa *rpc128-1007* SUP11 ura3 leu2-3, 112 ade2-1 lys2-1 trp *hxk1::HIS3MX6 hxk2::kanMX4*	This study
KR159-4D *hxk2Δ*	MATa SUP11 ura3 leu2-3, 112 ade2-1 lys2-1 trp *hxk2::kanMX4*	This study
KR159-4D *maf1Δ hxk2Δ*	MATa SUP11 ura3 leu2-3, 112 ade2-1 lys2-1 trp *maf1::URA3 hxk2::kanMX4*	This study
KR15-9C *hxk2Δ*	MATa *rpc128-1007* SUP11 ura3 leu2-3, 112 ade2-1 lys2-1 trp *hxk2::kanMX4*	This study
KR159-4D *hxk1Δ*	MATa SUP11 ura3 leu2-3, 112 ade2-1 lys2-1 trp	This study

bioRxiv preprint doi: https://doi.org/10.1101/372946; this version posted July 20, 2018. The copyright holder for this preprint (which was not certified by peer review) is the author/funder, who has granted bioRxiv a license to display the preprint in perpetuity. It is made available under aCC-BY 4.0 International license.

glk1Δ	*hxk1::HIS3MX6 glk1::kanMX4*	
KR159-4D *maf1Δ hxk1Δ glk1Δ*	MATa SUP11 ura3 leu2-3, 112 ade2-1 lys2-1 trp *maf1::URA3 hxk1::HIS3MX6 glk1::kanMX4*	This study
KR15-9C *hxk1Δ glk1Δ*	MATa *rpc128-1007* SUP11 ura3 leu2-3, 112 ade2-1 lys2-1 trp *hxk1::HIS3MX6 glk1::kanMX4*	This study
RS159-4D *glk1Δ*	MATa SUP11 ura3 leu2-3, 112 ade2-1 lys2-1 trp *glk1::kanMX4*	This study
RS159-4D *maf1Δ glk1Δ*	MATa SUP11 ura3 leu2-3, 112 ade2-1 lys2-1 trp *maf1::URA3 glk1::kanMX4*	This study
RS15-9C *glk1Δ*	MATa *rpc128-1007* SUP11 ura3 leu2-3, 112 ade2-1 lys2-1 trp *glk1::kanMX4*	This study
BY4741 *hxk2Δ*	MATa his3Δ1 leu2Δ0 met15Δ0 ura3Δ0 *hxk2::kanMX4*	Euroscarf
BY4741 *glk1Δ*	MATa his3Δ1 leu2Δ0 met15Δ0 ura3Δ0 glk1::kanMX4	Euroscarf
BY4741 *reg1Δ*	MATa his3Δ1 leu2Δ0 met15Δ0 ura3Δ0 reg1::kanMX4	Euroscarf
MB159-4D [pBM2636]	MATa SUP11 ura3 leu2-3, 112 ade2-1 lys2-1 trp [*HXT1::lacZ*]	This study
MB159-4D *maf1Δ* [pBM2636]	MATa SUP11 ura3 leu2-3, 112 ade2-1 lys2-1 trp *maf1::KanMX6*, [*HXT1::lacZ*]	This study
MB15-9C [pBM2636]	MATa *rpc128-1007* SUP11 ura3 leu2-3, 112 ade2-1 lys2-1 trp, [*HXT1::lacZ*]	This study

Proteomic analysis.

Samples (approx. 15 ml culture medium) - corresponding to 25 x 10^6 cells as determined in a cell count on hemocytometer were analysed by global label-free proteomics. Cells were spun down (10 min, 4°C) and the pellets flash frozen in liquid N_2 for storage. Cells were resuspended in 50 mM NH_4HCO_3, protease inhibitor

bioRxiv preprint doi: https://doi.org/10.1101/372946; this version posted July 20, 2018. The copyright holder for this preprint (which was not certified by peer review) is the author/funder, who has granted bioRxiv a license to display the preprint in perpetuity. It is made available under aCC-BY 4.0 International license.

ROCHE mini complete protease inhibitor. The samples were homogenized with MiniBeadbeater 24 (Biospec products) using the 200 µl of glass beads (425-600 µm; Sigma Aldrich) 15 times (3000 hits per min) with a duration of 30 s each with a 1 min cool down period in between each cycles. The cells were further centrifuged (10 min, 13000 rpm, 4°C). 250 µl fresh breaking-buffer was added to pellets and cells were washed by vigorous vortexing. The wash and cell debris were collected as flow through. Each flow through and supernatants from previous steps were combined. Protein concentration was determined with a Bradford assay [31].

A volume equivalent to 25 x 10^6 cells of each homogenate was removed, diluted with 25 mM AMBIC containing 0.05% Rapigest (Waters, Manchester) and shaken (550 rpm, 10 min, 80°C). The samples were then reduced (addition of 10 µl of 60 mM DTT and incubation at 60°C for 10 min) and alkylated (addition of 10 µl of 180 mM iodoacetamide and incubation at room temperature for 30 min in the dark). Trypsin (Sigma, Poole, UK, proteomics grade) was reconstituted in 50 mM acetic acid to a concentration of 0.2 µg/µl and 10 µl was added to the sample followed by overnight incubation at 37°C. The digestion was terminated and RapiGest™ removed by acidification (1 µl of TFA and incubation at 37°C for 45 min) and centrifugation (15,000 x g, 15 min). To check for complete digestion each sample was analyzed pre- and post-acidification by SDS-PAGE.

For LC-MS/MS analysis, a 2 µl injection of each digest, corresponding to approximately 25 x 10^4 cells, was analyzed using an Ultimate 3000 RSLC™ nano system (Thermo Scientific, Hemel Hempstead) coupled to a QExactive™ mass spectrometer (Thermo Scientific). The sample was loaded onto the trapping column (Thermo Scientific, PepMap100, C18, 300 µm X 5 mm), using partial loop injection, for 7 min at a flow rate of 4 µl/min with 0.1% (v/v) FA. The sample was resolved on the analytical column (Easy-Spray C18 75 µm x 500 mm 2 µm column) using a gradient of 97% A (99.9% water: 0.1% formic acid) 3% B (99.9% ACN: 0.1% formic acid) to 60% A: 40% B over 90 min at a flow rate of 300 nL min^{-1}. The data-dependent program used for data acquisition consisted of a 70,000 resolution full-scan MS scan (AGC set to $1e^6$ ions with a maximum fill time of 250 ms) the 10 most abundant peaks were selected for MS/MS using a 17,000 resolution scan (AGC set to $5e^4$ ions with a maximum fill time of 250 ms) with an ion selection window of 3 m/z and a normalised collision energy of 30. To avoid repeated selection of peptides for MS/MS the program used a 30 s dynamic exclusion window.

Label-free quantification.

bioRxiv preprint doi: https://doi.org/10.1101/372946; this version posted July 20, 2018. The copyright holder for this preprint (which was not certified by peer review) is the author/funder, who has granted bioRxiv a license to display the preprint in perpetuity. It is made available under aCC-BY 4.0 International license.

The raw data from the mass spectrometer was then processed using MaxQuant (MQ) software version 1.5.3.30 [32]. Protein identification was performed with the built-in Andromeda search engine, searching MS/MS spectra vs. the *S. cerevisiae* strain ATCC 204508/S288c downloaded from UniProt. (https://www.uniprot.org/proteomes/UP000002311). The following parameters were used; digest reagent: trypsin, maximum missed cleavages: 2, modifications: protein N-terminal acetylation and methionine oxidation, with a maximum of five modifications per peptide. The false discovery rate (FDR) for accepted peptide spectrum matches and protein matches was set to 1%. For protein quantification, the 'match between runs' options was selected. Label free quantification was performed with the MaxLFQ algorithm within MaxQuant (MQ), based on razor and unique peptides. All other MQ parameters were left at default values.

Protein significance testing.

To determine statistically significantly changing proteins with respect to the wild-type strain we used the MSstats package [33] in the R environment. Protein identities, conditions, biological replicates and intensities were directly uploaded from the MaxQuant output. Protein ID information was obtained from the 'proteinGroups.txt' file, conditions and biological replicates from the 'annotation.csv' file, and intensities from the 'evidence.txt' file. Data normalization was performed using the 'equalizeMedians' option and summarization using the Tukey's median polish option. Following this, a condition comparison was performed using the 'groupComparison' option from where the $\log_2$ fold changes and adjusted *p*-values were obtained.

Functional analysis.

Gene ontology enrichment analysis was performed with the online application Panther (34), directly on the Gene Ontology Consortium webpage (http://pantherdb.org/). The background set consisted of all proteins identified in a given MS experiment. Protein changes were mapped to central carbon and amino acid metabolic pathways following KEGG database [35] guidelines. Maf1 protein-protein interactions (PPI's) were obtained from the STRING [36] database and clustered with the Cytoscape [37] tool.

Transcription Factor target enrichment analysis

bioRxiv preprint doi: https://doi.org/10.1101/372946; this version posted July 20, 2018. The copyright holder for this preprint (which was not certified by peer review) is the author/funder, who has granted bioRxiv a license to display the preprint in perpetuity. It is made available under aCC-BY 4.0 International license.

For transcription factor (TF) target enrichment analysis, all proteins with an adjusted *p* value below 0.05 from both comparisons (WT - *rpc128-1007* and WT - *maf1Δ*) were uploaded to the GeneCodis tool [38]. Proteins were classified according to their positive or negative fold change and the background set consisted of all proteins identified in the given MS experiment. All statistical parameters were left as default. Adjusted *p*-values were obtained indicating those statistically significantly TFs being active according to their known target proteins.

Western blotting.

The total cellular proteins from Gcn4-3HA expressing yeast cells were extracted as described previously [27]. Protein extracts were separated by 12% SDS-PAGE and transferred to nitrocellulose membrane by electrotransfer (1 h, 400 mM, 4°C). For detection of HA-tagged proteins, monoclonal mouse anti-HA (1:3330, Sigma, H3663) and polyclonal goat anti-mouse antibodies (1:2000, Dako P0447) conjugated with horseradish peroxidase (HRP) were used. For Vma2 protein detection, monoclonal mouse anti-Vma2 antibodies (1:4000, Life Technologies, A6427) were used.

RNA isolation and RealTime PCR quantification.

RNA isolation and real-time PCR amplification was performed as described previously [27]. Isolated RNAs were examined by SYBR GREEN-based Real-time PCR. Oligonucleotide sequences of the primers used in Real-time PCR experiment for *GCN4* were taken from Cankorur-Cetinkaya *et al.* [39]. Samples were normalized to two reference genes - *U2* spliceosomal RNA (*U2*) and small cytosolic RNA (*SCR1*). Expression levels in WT strain (MB159-4D) was taken as 1.0. The relative expression (mean±SD) were calculated for at least three independent biological replicates. Statistical significance of *p*-values were determined by t-student test.

Enzymatic assays.

All yeast strains including transformants carrying *pBM2636* plasmid [40] for measurement of β-galactosidase activity were cultivated in rich medium supplemented with 2% glucose (YPD) or 2% glycerol (YPGly) at 30°C with agitation of 250 rpm until reached $A_{600} \approx 1.0$. Yeast cultures were harvested at 5000 rpm at 4°C and washed twice with 10 mM potassium phosphate buffer, pH = 7.5. Cells for Hxk, Pgk1, Cdc19 and Zwf1 activity

bioRxiv preprint doi: https://doi.org/10.1101/372946; this version posted July 20, 2018. The copyright holder for this preprint (which was not certified by peer review) is the author/funder, who has granted bioRxiv a license to display the preprint in perpetuity. It is made available under aCC-BY 4.0 International license.

196 assays were suspended in 100 mM KPi pH = 7.5, for β-galactosidase in 50 mM potassium phosphate buffer pH =
197 7.0, rapidly frozen in liquid nitrogen and stored at -20°C. Samples were washed twice with sonication buffer
198 (100 mM potassium phosphate buffer, pH = 7.5, 2 mM $MgCl_2$) or 50 mM potassium phosphate buffer pH = 7.0
199 in the second case and disintegrated with Mini-Beadbeater 24 (Biospec products) using glass beads (425–
200 600 µm; Sigma Aldrich). Hexokinase (EC 2.7.1.1) activity was measured according to Adamczyk [41],
201 phosphoglycerate kinase (Pgk1, EC 2.7.2.3) according to De Winde *et al* [42], pyruvate kinase (Cdc19; EC
202 2.7.1.40) according to Gruning *et al* [43], glucose-6-phosphate dehydrogenase (Zwf1, EC 1.1.1.49) according to
203 Postma *et al.* [44], β-galactosidase according to Smale 2010 (45), and catalase (EC 1.11.1.6) according to Beers
204 and Sizer [46]. All assays were performed for at least three independent biological replicates.
205

206 **Glycogen, trehalose and fructose 1,6 bisphosphate measurement.**

207 The glycogen and trehalose content was measured in yeast cells, grown in YPD until $A_{600} \approx 1.0$. Cell preparation
208 and extraction was as described in Rossouw *et al.* 2013 [47]. Glycogen determination was as described by
209 Parrou and Francois [48]. Glucose concentration from glycogen enzymatic breakdown was determined by the
210 glucose (HK) Assay Kit according to the manufacturer's protocol (Sigma Aldrich, GAHK-20). Trehalose content
211 was measured using Trehalose Assay Kit (Megazyme International Ireland, Wicklow, Ireland) according to
212 manufacturer's protocol. Fructose 1,6 bisphosphate was measured according to Peeters *et al.* (2017) [4] with
213 minor modifications.
214

215 **Determination of yeast fermentative capacity.**

216 Fermentative capacity assays were performed as described by van Hoek *et al.* [49] with minor changes. The
217 fermentative capacity can be defined as the specific maximal production rate of ethanol per gram of biomass
218 (mmol/g/h) under anaerobic conditions at excess of glucose. Samples corresponding to 60-70 mg dry weight
219 were harvested by centrifugation at 5000 rpm at 4°C. Cells were washed twice with synthetic medium CBS-
220 without carbon source and resuspended in CBS (-C) to make 2% wet weight suspensions. Analysis was
221 performed in a thermostatted (30°C) vessel. Cells were flushed with N_2 gas at a flow rate of approximately
222 0.6 L/h and glucose was added to a final concentration of 10 g/liter. Samples for measurement of ethanol were
223 collected every 5 min incubated with 35% (w/v) perchloric acid on ice for 10 min and neutralized with KOH

bioRxiv preprint doi: https://doi.org/10.1101/372946; this version posted July 20, 2018. The copyright holder for this preprint (which was not certified by peer review) is the author/funder, who has granted bioRxiv a license to display the preprint in perpetuity. It is made available under aCC-BY 4.0 International license.

224 before centrifugation at 13000 rpm and stored in -20°C freezer. The ethanol production of each strain was
225 normalized to the dry weight of the culture. Ethanol and glycerol in supernatants were determined with
226 enzymatic assays according to manufacturer (Megazyme).
227
228 **Biomass determination.**
229 Sample suspensions of 1 ml volume in duplicates were filtered over pre-weighted nitrocellulose filters (pore
230 size, 0.45 µm; HAWP04700). After removal of medium, the filters were washed with demineralized water, dried
231 in an oven overnight and weighted [49].
232

bioRxiv preprint doi: https://doi.org/10.1101/372946; this version posted July 20, 2018. The copyright holder for this preprint (which was not certified by peer review) is the author/funder, who has granted bioRxiv a license to display the preprint in perpetuity. It is made available under aCC-BY 4.0 International license.

Results

Overall proteome profiling and changes

We hypothesized that perturbations in RNAP III activity would impact on global expression of the proteome. The lack of the negative regulator of RNAP III, Maf1, as well as the loss of function due to a point mutation in the RNAP III *RET1*/C128 subunit, would be expected to elicit broad changes in the *Saccharomyces cerevisiae* proteome. We aimed to identify proteins, the changed abundance of which, could explain the diminished growth of *rpc128-1007* on glucose and de-repression of *HXT2 and HXT6/7* genes that encode high affinity glucose transporters, when compared to *maf1Δ* under glucose rich conditions [27]. To examine the phenomenon we performed a systematic comparative analysis of *maf1Δ* and *rpc128-1007* mutants using label-free proteomics.

Reproducible, deep proteome coverage was obtained (Fig 2 A) for *maf1Δ* and *rpc128-1007* mutants grown under glucose rich conditions. The proteomics data were of high quality, with replicates clustered together and no systematic difference reflecting sample preparation bias (Fig 2). In total, over 2,300 protein groups were identified and quantified. As anticipated, there was considerable overlap between the *maf1Δ* and *rpc128-1007* proteomes (Fig 3). Differential proteome analysis was carried out pairwise in two sets as follows: WT *vs rpc128-1007* mutant and WT *vs maf1Δ* mutant, resulting in 2,294 quantified proteins common to all strains. A subset of statistically significant changes revealed 249 proteins that were common to both comparisons (with an adjusted p-value < 0.05). This subset of 249 proteins were clustered into coherent groups (see Material and Methods) which display common Gene Ontology (GO) annotation, consistent with coordinated regulation of relevant biological processes (Fig 3 B). Some of the groups exhibited parallel changes in the two strains (Groups 1-4) whereas others highlighted divergent, essentially reciprocal, functions in the two strain (i.e. Groups 5–6). These unbiased clusters show enrichments for concerted biological functions, embodied by the limited subset of GO term enrichments listed in Fig 3B, including elements of amino acid and monosaccharide/carbohydrate metabolism. In both strains, enzymes of gluconeogenesis and the glyoxylate cycle were *decreased* when compared to the reference strain grown under the same glucose repression conditions (Group 2). Groups 7 and 9 also show decreased protein abundance with respect to wild type, and are similarly enriched in enzymes from the TCA cycle, purine ribonucleotide biosynthetic pathways, *de novo* inosine monophosphate

bioRxiv preprint doi: https://doi.org/10.1101/372946; this version posted July 20, 2018. The copyright holder for this preprint (which was not certified by peer review) is the author/funder, who has granted bioRxiv a license to display the preprint in perpetuity. It is made available under aCC-BY 4.0 International license.

biosynthesis, and also mitochondrial transmembrane transport. In contrast, many of the enzymes involved in *de novo* amino acid synthesis were increased in abundance in both *maf1Δ* and *rpc128-1007* (Groups 1, 3, 4). The negatively correlated, reciprocally altered groups (Groups 5, 6 and 8) were consistent with shifts in trehalose biosynthesis, pentose phosphate pathway (PPP) activity, oxidative stress, oxidation-reduction processes, glycine catabolic processes, replicative cell aging and alcohol production.

Key enzymes of the glyoxylate cycle are reduced in abundance in both *maf1Δ* and *rpc128-1007* mutants.

In both strains phosphoenolpyruvate carboxykinase (Pck1) and malate synthase 1 (Mls1) were reduced (Fig 4). These enzymes direct acetyl-CoA to malate and oxaloacetate that in turn can be metabolized to phosphoenolpyruvate for gluconeogenesis. The enzymes are components of the glyoxylate cycle that allows yeast cells to metabolize non-fermentable carbon sources, including fatty acids. The mechanism governing glucose repressed genes is particularly important in the RNAP III compromised mutant as well as in Maf1 deprived cells due to the previously reported growth perturbations of *maf1Δ* on non-fermentable carbon source. 2-fold decrease in *maf1Δ PCK1* mRNA was reported [26], though under inducing conditions on glycerol. Notably, the relative decrease in Pck1 abundance in Maf1 deficient cells is the largest in our proteomic dataset. The very much decreased Pck1 abundance proves that the enzyme is subject to degradation in a glucose-dependent manner [50] and the mechanism is not perturbed in both the mutants. Other enzymes of the glyoxylate cycle, are concomitantly reduced in *maf1Δ* cells, including malate dehydrogenases Mdh2, Mdh3, isocitrate lyase (Icl1) and glyoxylate aminotransferase (Agx1), the last implicated in glycine synthesis from glyoxylate. In *rpc128-1007*, most of the glyoxylate enzymes as well as those of the TCA cycle were also decreased. Enzymes of the TCA and glyoxylate cycles undergo coordinated transcriptional down regulation [50,51] induced by glucose through the master kinase Snf1/AMPK [52,53] therefore strongly suggesting unperturbed functioning of Snf1 signaling on glucose. In contrast, the other key enzyme of gluconeogenesis, Fbp1 (fructose 1,6 bisphosphatase) that bypasses the physiologically irreversible step in the glycolytic pathway, was increased under glucose deprivation in *maf1Δ*, but was unchanged in *rpc128-1007* mutant.

bioRxiv preprint doi: https://doi.org/10.1101/372946; this version posted July 20, 2018. The copyright holder for this preprint (which was not certified by peer review) is the author/funder, who has granted bioRxiv a license to display the preprint in perpetuity. It is made available under aCC-BY 4.0 International license.

Reduction in glycolytic enzymes in a RNAP III compromised strain correlates with lower activity of the glucose transporter Hxt1.

Proteome analysis captured changes in relative cellular abundances of all glycolytic enzymes and implied a reduced capacity for glycolysis in *rpc128-1007* cells, but an unchanged glycolytic capacity in *maf1Δ* cells (Fig 4). In *rpc128-1007,* enzymes that were significantly decreased (between 2- and 2.6-fold) included glyceraldehyde-3-phosphate dehydrogenase isozyme 1 (Tdh1), enolase (Eno1), glyceraldehyde-3-phophate dehydrogenase isozyme 2 (Tdh2), 3-phosphoglycerate kinase (Pgk1) and glucokinase (Glk1). The lower abundance of the entire complement of glycolytic enzymes is consistent with reduced glycolytic performance in *rpc128-1007*.

Glycolytic flux in *S. cerevisiae* can regulate glucose uptake, at least in part through the activity of glucose uptake mechanisms [54] and in particular, induction and increases of membrane internalization of low-affinity glucose transporters [40,55–58]. The principal example is Hxt1, only activated when yeast grow in glucose rich media [40]. We explored the potential for changes in glucose transport by measurement of transcriptional de-repression of the key gene encoding the major low affinity, high capacity glucose transporter *HXT1,* in *maf1Δ* and *rpc128-1007* using a *HXT1-lacZ* reporter plasmid (Fig 5 B). The *HXT1* gene was strongly activated in *maf1Δ* under glucose rich conditions, whereas a 3-fold lower activity of the *HXT1* promoter was observed in *rpc128-1007* cells in the same conditions. When assessed in cells grown on glycerol, expression of *HXT1–lacZ* reporter was decreased in all strains (Fig 5 B) as expected [40]. Consistent with the reports on mutants in genes of the glycolytic pathway, which are blocked in glycolysis [59], the *HXT1* expression was reduced in RNAP III compromised yeast suggesting that in this mutant, supply of glucose for a functional glycolytic pathway cannot be maintained.

Positive relationship between Hxk2, Tdh and Cdc19 enzyme activities and the potency of RNAP III dependent transcription.

Since *HXT1* gene expression was elevated in *maf1Δ,* but decreased in *rpc128-1007,* we measured the activity of selected glycolytic enzymes *in vitro* [41] in both mutant strains and evaluated the relationship between activity changes and changes in protein abundance assessed by proteomics. *S. cerevisiae* encodes three isoenzymes with hexokinase activity (Fig 5 A). Proteomic analysis suggested that Glk1 was the isoenzyme phosphorylating

bioRxiv preprint doi: https://doi.org/10.1101/372946; this version posted July 20, 2018. The copyright holder for this preprint (which was not certified by peer review) is the author/funder, who has granted bioRxiv a license to display the preprint in perpetuity. It is made available under aCC-BY 4.0 International license.

316 glucose in *maf1Δ* (Fig 4), with increased abundance whereas Hxk1 and Hxk2 were observed decreased in this
317 strain. For *rpc128-1007*, the protein abundance of all enzymes conferring hexokinase activity was decreased
318 (Fig 4). We therefore grew the three strains in rich media supplemented with 2% (w/v) glucose and measured
319 the hexokinase reaction (V_{max}) in cell free extracts. Total hexokinase activity was increased in *maf1Δ* and
320 reduced in *rpc128-1007* (Fig 5 C, solid bars).
321
322 To quantify the activities of the individual hexokinase enzymes we designed and constructed deletion mutants
323 of hexokinases in the three strains (Fig 5 C, D). Quantification of glucose phosphorylation activity in single and
324 double null mutants of genes encoding hexokinases clarifies that hexokinase 2 (Hxk2) is the predominant
325 isoenzyme engaged in glucose phosphorylation in *maf1Δ*. The triple deletion *maf1Δ hxk1Δ glk1Δ*, in which the
326 only isoform left intact is Hxk2, results in comparable hexokinase activity to the observed in *maf1Δ* deletion
327 strain with all the isoforms present (Fig 5 C). In contrast, the mutants in whom we observe the reverse trend in
328 the enzymatic activity, are the *maf1Δ hxk2Δ* double mutant and *maf1Δ hxk1Δ hxk2Δ* triple mutant. An increase
329 in glycolytic flux is possible to achieve in cells lacking Maf1 despite a decrease in Hxk2 abundance and only a
330 slight increase in Glk1 cellular concentration. Under growth on glycerol, there was an increased contribution of
331 Hxk1 to total hexokinase activity in wild-type, *maf1Δ* and *rpc128-1007* (Fig 5 D), suggesting that the
332 compensation regulatory mechanisms are not perturbed in the two mutant strains. *HXK1* induction by non-
333 fermentable carbon source has previously been reported [60]. Interestingly, on glycerol growth, the total
334 hexokinase activity in *rpc128-1007* was higher than in *maf1Δ*.
335
336 Since glyceraldehyde-3-phoshate dehydrogenase (Tdh) and pyruvate kinase (Cdc19) are important providers of
337 NADH and ATP respectively, these enzymes were also assayed. Measuring the activity of controlling and rate-
338 limiting glycolytic enzymes is one of the techniques to estimate carbon flux thought the entire pathway. In
339 yeast, glyceraldehyde-3-phoshate dehydrogenase, placed between upper and lower segments of glycolysis, is
340 considered a rate controlling step of glycolysis [61,62] whereas Cdc19 kinase levels affect the rate of carbon
341 flux and its direction towards pyruvate (PYR) or phosphoenolpyruvate (PEP) under fermentative conditions. The
342 activity of Cdc19 is sufficient to cause a shift from fermentative to oxidative metabolism in *S. cerevisiae* [43,63]
343 and controls glycolytic rate during growth on glucose [64].
344

bioRxiv preprint doi: https://doi.org/10.1101/372946; this version posted July 20, 2018. The copyright holder for this preprint (which was not certified by peer review) is the author/funder, who has granted bioRxiv a license to display the preprint in perpetuity. It is made available under aCC-BY 4.0 International license.

In *maf1Δ*, in which there was a small increase of Tdh1, 2 abundance (Tdh1; 0.21 log_2FC and 0.3 adj. *p* value, Tdh2: 0.16 log_2FC and 0.37 adj. *p* value), *in vitro* activity was 2-fold higher (Fig 5 E). From proteomics, Tdh activity was slightly lower in *rpc128-1007* cells under the same growth conditions, but Tdh activity measured in *rpc128-1007* grown on glycerol was significantly lower when compared to the reference strain, which suggests that the catalytic activity of the enzyme decreases *in vivo* while the enzyme converts 1,3-bisphosphoglycerate (1,3-BPG) into glyceraldehydes-3-phosphate (G3P) in the reverse direction to glycolysis, when the enzymes is involved in gluconeogenesis in the presence of non-fermentable carbon sources in the medium. This shuttle between the cytosol and the nucleus linking metabolic redox status to gene transcription [65] and contributes to tRNA transport [66].

We further measured activity of the final enzyme in the glycolytic pathway, pyruvate kinase (Cdc19) activity. Cdc19 concentration is comparable in *maf1Δ* and its parental strain. We found (Fig 5 F), that Cdc19 shows significantly lower enzymatic activity in *rpc128-1007* compared to the reference strain grown on glucose, but a slightly elevated activity in Maf1 deficient cells both on glucose and glycerol. Overall, in *maf1Δ* the glycolytic enzymes show higher activity than originally thought judging by proteomics data, whereas Hxk2, Tdh and Cdc19 protein decreased abundance in *rpc128-1007* is fully in agreement with their reduced enzymatic activity. This lead us to the conclusion that glycolytic flux is diminished in *rpc128-1007*, whereas in *maf1Δ* it is not only higher than in *rpc128-1007* but also in WT. Due to the fact that F16BP mediated allosteric control [67–69], but not Cdc19 abundance or phosphorylation, was reported as having a predominant role in regulating the metabolic flux through the pyruvate kinase Cdc19 [70]. Therefore, we measured F16BP intracellular concentration.

Fructose 1,6 bisphosphate intracellular concentration does not reflect differences in RNAP III activity and glycolytic flux in the mutant strains.

The glycolytic metabolite F16BP is a molecule triggering of the metabolic switch from respiration to fermentation in unicellular and higher organisms [3,4,64]. We reasoned that lower glycolytic flux in *rpc128-1007*, would result in lower fructose 1,6 bisphosphate (F16BP) concentration in this mutant. We measured F16BP in *rpc128-1007* grown under anaerobic conditions. After addition of 100 mM glucose, F16BP

bioRxiv preprint doi: https://doi.org/10.1101/372946; this version posted July 20, 2018. The copyright holder for this preprint (which was not certified by peer review) is the author/funder, who has granted bioRxiv a license to display the preprint in perpetuity. It is made available under aCC-BY 4.0 International license.

concentration sharply increased during the first two minutes to the physiological level observed in the wild-type cells but then declines to a new steady state. In *maf1Δ* cells, the concentration of F16BP is similar to *rpc128-1007* but there is no initial overshoot (Fig 6). The intracellular level of F16BP is therefore unlikely to be the trigger for the perturbed metabolic switching in cells with different RNAP III activity. Another product of glycolysis (or its side branches) may control the transcriptional reprogramming in yeast, particularly when there are multiple-metabolite-responsive elements present at promoters to sense diverse metabolic signals. Additionally, F16BP concentration may affect Cdc19 activity *in vivo,* thus the flux direction.

Higher glucose flux in Maf1 deficient cells results in activation of glycogen and trehalose shunts.

We explored the direction of carbon flux in *maf1Δ* in the absence of any increase in F16BP concentration. Yeast cells are equipped to counteract excessive influx of glucose by diversion of glucose into glycogen and trehalose [71]. During exponential growth, glycogen and trehalose biosynthesis play additional roles as part of an adaptive response facilitating survival when the cell is challenged with increased glycolytic flux as a consequence of glucose overflux into a cell. The glycogen shunt prevents accumulation of glycolytic intermediates, particularly F16BP and ATP that otherwise would ultimately lead to perturbation in cell metabolic homeostasis [72–75].

The proteomics data confirmed a strong, negative correlation between RNAP III activity and enzyme abundance in the trehalose and glycogen synthesis pathways, which share common enzymes. UDP-glucose pyrophosphorylase (Ugp1), trehalose-6-P synthases (Tps1 and Tps2) and glycogen synthase (Gsy2) increase in *maf1Δ,* whilst the same proteins were markedly reduced in *rpc128-1007* cells (Fig 3, group 6, Fig 4). The product of Tps1 activity, trehalose-6-phosphate, controls glycolysis by restricting the flow of glucose into the pathway and is an allosteric inhibitor of hexokinase 2 activity [72,76]. We assessed the metabolic allocation of glucose through quantification of trehalose and glycogen content during exponential growth. Both metabolites were 2.5-fold higher in *maf1Δ* in the presence of high glucose. By contrast, *rpc128-1007* cells could accumulate neither glycogen nor trehalose (Fig 7 A and B).

bioRxiv preprint doi: https://doi.org/10.1101/372946; this version posted July 20, 2018. The copyright holder for this preprint (which was not certified by peer review) is the author/funder, who has granted bioRxiv a license to display the preprint in perpetuity. It is made available under aCC-BY 4.0 International license.

In summary, the results are consistent with increased glycolytic flux in *maf1Δ* and conversely, a diminished flux in *rpc128-1007*. Metabolic overflow in *maf1Δ* leads to flux redistribution into the trehalose pathway, to protect the cells from either an increase in intracellular glucose concentration or accumulation of glycolytic intermediates downstream from glucose-6-phosphate as observed in wild-type budding yeast [77].

Ethanol overproduction is not observed in cells lacking Maf1 during logarithmic growth.

In yeast, glucose is fermented to ethanol for energy production, as it is often used as a measure of increased glycolytic flux. We examined, whether *maf1Δ* produces ethanol more efficiently than the wild type, as might be predicted from the Group 8 GO terms (Fig 2). Pyruvate decarboxylases isoenzymes Pdc5 and Pdc6 (the key enzymes in alcohol fermentation) are increased in abundance in *maf1Δ* (1.7 and 2.3 Log_2FC respectively), suggested that Maf1 deficiency should lead to increased ethanol synthesis. We performed a fermentative capacity assay under anaerobic conditions; without cells pretreatment or with the pretreatment, when cells were glucose starved for 10 min. Under both condition there was no evidence of enhanced ethanol production in *maf1Δ* (Fig 7 C, S1 Table). Instead, accumulation of the fermentation by-product, glycerol was observed (Fig 7 D). This is consistent with increased glycolytic flux being rerouted upstream of pyruvate or downstream from acetaldehyde by the enzymes of the pyruvate dehydrogenase bypass [49].

Glycerol rather than ethanol production was also evident under aerobic conditions suggesting that access to oxygen does not affect the glycolytic flux redirection towards glycerol biosynthetic pathway in *maf1Δ*. The *maf1Δ* mutant is possibly under oxidative stress, since glycerol production has a role in response to the stress. Evidence for oxidative stress in *maf1Δ* also derives from increased protein abundance for the pentose phosphate pathway (PPP) enzymes in this mutant, which balances the systemic manifestation of reactive oxygen species and the ability to detoxify reactive intermediates [78].

Activation of pentose phosphate pathway in cells deprived of Maf1 regulator.

The comparative proteomic analysis suggests reciprocal modulation of the pentose phosphate pathway (PPP), in *rpc128-1007* and *maf1Δ* (Figs 4, 8). PPP is a source of NADPH during oxidative stress conditions. The data are consistent with an increase in flux through the PPP in *maf1Δ,* which can be achieved by increased glucose-6-

bioRxiv preprint doi: https://doi.org/10.1101/372946; this version posted July 20, 2018. The copyright holder for this preprint (which was not certified by peer review) is the author/funder, who has granted bioRxiv a license to display the preprint in perpetuity. It is made available under aCC-BY 4.0 International license.

phosphate dehydrogenase Zwf1 abundance, the enzyme catalyzing the rate limiting, irreversible step of the pathway. Downstream enzymes including 6-phosphogluconolactonase (Sol3, Sol4) and 6-phosphogluconate dehydrogenase Gnd2 that balance the redox potential *via* the cytosolic NADPH/$NADP^+$ ratio in native yeast cells and both isoforms of transketolase (Tkl1, Tkl2) are increased in *maf1Δ*. Conversely, depletion of Zwf1, Sol4 Tkl1 and Tkl2 in *rpc128-1007* is consistent with a reduced potential of this mutant to redirect carbon flux from glucose-6-phosphate (G6P) towards 6-phosphogluconolactone (6PG) and downstream metabolic intermediates (Figs 4, 8).

We grew yeast in rich medium supplemented with 2% glucose as previously and measured the Zwf1 glucose-6-phosphate dehydrogenase reaction rates (V_{max}) in cell free extracts to check the potential to produce NADPH. This enzyme is highly regulated and is critical in determining the overall flow of glucose into the pentose phosphate pathway [79,80]. Zwf1 activity in *maf1Δ,* was elevated not only on glucose, as carbon source but also using glycerol whereas the activity in *rpc128-1007* remains essentially unchanged (S1 A Fig). To further corroborate the relationship between *MAF1* deletion and the oxidative stress response other proteins, such as Ctt1 stress inducible cytosolic catalase T were elevated (S2 Table). Further, total catalase activity was higher in *maf1Δ,* when compared to WT or *rpc128-1007* (S1 B Fig). The magnitude of the abundance changes in enzymes of the oxidative stress response, is observed during carbon source downshift. Here however, it occurs in the presence of glucose during the exponential phase, indicates that *MAF1* gene deletion elicits broader metabolic reprogramming than originally thought.

RNAP III subunit *RET1*/C128 point mutation is associated with metabolic reprogramming dependent on transcriptional and translational induction by Gcn4.

Glycolytic intermediates are precursors of the carbon skeletons of several amino acids. Thus, lowered glucose flux could result in the amino acid starvation response in yeast. We identified a large group of proteins that were substantially increased in abundance, that are involved in amino acid biosynthesis. The relative abundance of those was increased in *rpc128-1007* relative to WT. However, the same set of enzymes in *maf1Δ* were increased in some cases and unchanged in others. The magnitude of the increases were generally much higher in the *rpc128-1007* compared to the *maf1Δ* mutant. In *rpc128-1007,* over 30 proteins in the pathways

bioRxiv preprint doi: https://doi.org/10.1101/372946; this version posted July 20, 2018. The copyright holder for this preprint (which was not certified by peer review) is the author/funder, who has granted bioRxiv a license to display the preprint in perpetuity. It is made available under aCC-BY 4.0 International license.

for arginine, lysine, leucine, isoleucine, and valine biosynthesis *de novo,* along with aromatic amino acids such as histidine, tryptophan, tyrosine and threonine or their precursors were elevated (Fig 8).

In *rpc128-1007,* the decreased cellular concentration was observed in methionine biosynthesis subpathway, that is for ATP sulfurylase the product of *MET3* gene essential to catalyse the first step for assimilatory reduction of sulfate to sulfide, involved in methionine metabolism. The other proteins diminished in *rpc128-1007* were Ser3, Ser33, Cys3 and Shm2 contributing to serine and cysteine biosynthesis.

In *maf1Δ,* the proteins Arg4, Arg3, Cpa2, Bat1, Bat2, Leu1, Leu4, Leu9 and Ilv3 were elevated; all are components of the metabolic branch that is part of L-arginine and L-leucine biosynthesis (Fig 8). By contrast *rpc128-1007, maf1Δ* cells exhibited enrichment in the branch of serine/cysteine, methionine biosynthesis pathway and sulfate metabolism (Met3, Met5, Met10, Met14), and these abundance changes were amongst the largest in the proteomic dataset. The expression of most genes involved in amino acid biosynthesis is under the control of the Gcn4 transcriptional activator, part of the general amino acids control (GAAC) regulon [81,82]. *GCN4* transcription is stimulated by starvation for amino acids, purine, glucose limitation and specifically by initiator $tRNA^{Met}$ depletion [83,84]. Therefore, we evaluated the mRNA levels of *GCN4* by RT-PCR (Fig 9 A).

The *GCN4* mRNA steady state levels were 11-fold higher in the *rpc128-1007* and, 2-fold elevated in *maf1Δ.* The difference between these two mutants is reflected in the extent of the response in the proteomics analysis *rpc128-1007* had much stronger phenotypic change than *maf1Δ.* We constructed mutant strains with chromosomally encoded *GCN4-3HA* protein fusions to assess Gcn4 protein abundance by immunoblotting. Gcn4 abundance, normalized to Vma2 level in the total protein extracts, was elevated 3-fold in *rpc128-1007* and 2-fold in *maf1Δ,* when compared to the reference strain (Fig 9 B, C). The marked decoupling between transcript and protein changes in the strains, *rpc128-1007* (11-fold mRNA, 3-fold protein) and *maf1Δ,* (2-fold mRNA, 2-fold protein), also suggests that other regulatory factors are in operation.

For the entire proteome data set, we were able to perform transcription factor enrichment analysis, using the web-based GeneCodis tool to identify over-representation of the targets of given transcription factors in the

bioRxiv preprint doi: https://doi.org/10.1101/372946; this version posted July 20, 2018. The copyright holder for this preprint (which was not certified by peer review) is the author/funder, who has granted bioRxiv a license to display the preprint in perpetuity. It is made available under aCC-BY 4.0 International license.

differentially abundant proteomes (Fig 10). For *rpc128-1007,* Gcn4 was the predominant transcription factor. highlighted by the analysis for gene activation. The second most predominant transcriptional factor was Leu3 (S2 Fig) followed by Yap1 and Bas1. We also identified a group of genes with motifs enriched for GATA transcriptional factors such as Dal81, Dal80 and Gzf3 regulating genes by nitrogen catabolite repression (NCR).

The outcome of experimental and *in silico* analyses is that the dramatic increase in specific protein changes observed in *rpc128-1007* can be largely attributed to the *GCN4* stress response and *GCN4* de-repression on glucose. By contrast to the highly focused changes in *rpc128-1007,* the gene regulatory network in *maf1Δ,* (which liberates RNAP III from regulatory circuits and nutrient signaling) (Fig 1), exhibits a broad spectrum of modest changes (including more balanced *GCN4* up-regulation) across several cellular processes, to provide the mutant with better adaptation/selective advantage to growth in glucose-rich environment.

Discussion

Regulation of the central carbon metabolism of *S. cerevisiae* has always been a topic of considerable interest. Here, we present for the first time, the evidence that glycolytic flux in yeast can be modulated accordingly to the RNAP III activity and that central carbon metabolism adjusts to the activity of RNAP III in yeast. Our results clearly indicate the new connections between RNAP III and cellular metabolism. On the basis of the previous and the present findings, we propose that there is an internal signaling in the yeast cells, that competes against the extracellular nutrients-sensing, when a cell faces non-optimal RNAP III activity.

An RNAP III point mutation in the *RET1*/C128 subunit is correlated with lower efficiency of glycolysis and up-regulation of *GCN4* dependent genes of amino acid metabolism.

In a previous report we have shown that the *rpc128-1007* strain is insensitive to external glucose concentration cues, which manifests *via* constitutive overexpression of the *HXT2* gene, whether in glucose or glycerol growth conditions [27]. Our new data suggest that the *rpc128-1007* mutant operates under substrate limitation, such as glucose, even though the sugar is present in excess in the growth medium. RNAP III activity inhibition results in diminished abundance of enzymes in central carbon metabolism and elicits preferential synthesis of proteins involved in amino acids biosynthesis (Fig 8) attributable to the *GCN4* response. Gcn4 is translationally up-

bioRxiv preprint doi: https://doi.org/10.1101/372946; this version posted July 20, 2018. The copyright holder for this preprint (which was not certified by peer review) is the author/funder, who has granted bioRxiv a license to display the preprint in perpetuity. It is made available under aCC-BY 4.0 International license.

514 regulated in response to numerous tRNA perturbations [84,85] and yeast cells with the *RET1*/C128 point
515 mutation produce as much as 1.6-fold less tRNA molecules compared to WT. This suppresses the defect of
516 Maf1 inactivation, caused by increased or unbalanced levels of various tRNAs including increased $tRNA^{Met}$ levels
517 [13]. Initiator $tRNA^{Met}$ depletion triggers a *GCN4*-dependent reprogramming of global genome expression in
518 response to decreased RNAP III transcription in *rpc160-112* mutant (in the largest C160 subunit) [84]. However,
519 *HXT2* transcription is not dependent on Gcn4 transcriptional activity [84] in the *rpc160-122* mutant. *HXT2*
520 overexpression in *rpc128-1007* is most likely related to lower glycolytic efficiency in the mutant strain [59], but
521 the direct regulator of the phenomenon still remains to be discovered.
522
523 In the wild-type yeast cells, most glycolytic enzymes exist with significant overcapacity, regardless the carbon
524 source. The enzymes are present in the cells at generally fixed concentration, even if reverse glycolytic
525 processes take place [86]. However, in the *rpc128-1007* mutant, the abundance of all the glycolytic isoenzymes
526 is reduced and concomitantly with a decrease in abundance of several proteins engaged in the side branches of
527 the glycolytic pathway (trehalose/glycogen shunt and PP pathway). The two enzymes, fructose 1,6
528 bisphosphatase Fbp1 and pyruvate kinase 2 Pyk2, that catalyze the reactions in gluconeogenesis are the least
529 affected in *rpc128-1007* in agreement with the preference of this mutant to grow on respiratory carbon
530 sources such as glycerol [13].
531
532 In a *Drosophila melanogaster* gut model [87], reduction of RNAP III activity through controlled degradation of
533 the C160 subunit (C160 encoded by *RPC160)* leads to diminished protein synthesis. Inhibition of RNAP III affects
534 RNAP I, but not RNAP II-generated transcripts, suggesting that translation is the major factor regulating protein
535 abundance in RNAP III compromised cells [87]. This further suggests that the *rpc128-1007* mutant might be
536 limited at translation and indeed, the *rpc128-1007* mutant has reduced tRNA levels [13]. In *rpc128-1007,*
537 translation seems to be selective towards enzymes in *de novo* amino acids synthesis at the expense of the full
538 complement of glycolytic enzymes. As a consequence of decreased abundance of the glycolytic enzymes, the
539 glycolytic flux is very likely to decrease. Proteins could also be selectively stabilized in the *rpc128-1007*
540 background. This accords with our finding that in *rpc128-1007* there is a decrease in RPN4 regulated elements
541 of the protein degradation machinery, including the 26S proteasome genes [88,89] (Fig 10, S3 Table). As a
542 result, an increase resistance to proteostatic challenge in this mutant could ensue (Fig 10). High turnover

bioRxiv preprint doi: https://doi.org/10.1101/372946; this version posted July 20, 2018. The copyright holder for this preprint (which was not certified by peer review) is the author/funder, who has granted bioRxiv a license to display the preprint in perpetuity. It is made available under aCC-BY 4.0 International license.

proteins may be stabilized even in an environment of diminished protein synthesis in *rpc128-1007* [90]. Overall reduction of protein catabolism might be critical for survival, consistent with a high enrichment of down-regulated proteins in this genetic background. The reduction of abundance of selected glycolytic enzymes, such as Hxk2, Tdh and Cdc19 in *rpc129-1007* is followed by the decrease in their enzymatic activity at high concentrations of glucose (Figs 5 and 6). Lowering the intracellular Cdc19 concentration is sufficient to shift from fermentative to oxidative metabolism in yeast, which reduced flux towards pyruvate [43]. The lower abundance and activity of the first (Hxk2) and the last (Cdc19) enzymes in the glycolytic pathway can be expected to reduce glycolytic flux in the mutant.

The RNAP III *RET1*/C128 mutation elicits a diminution of the low affinity glucose transporter 1 (activated on high glucose), the major glucose transporter facilitating glucose uptake under glucose rich conditions [56] and which is under control of Rgt2 (low affinity) glucose sensor (Fig 5B). External glucose signaling, may not be a dominant factor in reprogram *HXT* genes expression in *rpc128-1007*, glucose metabolism may dominate in this case [27]. Our data are consistent with the postulate that "glucose" sensing could occur intracellularly [1–4], but not yet (so far) linked to metabolic reprogramming upon change in RNAP III activity. There is some debate as to whether the signaling molecule for metabolism switching is fructose 1,6 bisphosphate [4,56]. F16BP triggers a switch in metabolism from respiration to fermentation in unicellular and higher organisms. It is the key metabolic factor determining AMPK/Snf1 kinase activity and is a potent activator of Ras pathway [3,4,64]. If F16BP plays such key roles, we reasoned that the intracellular concentration should be lower *rpc128-1007* and higher in *maf1Δ*.

Although significantly lower than in the wild-type cells, the levels of F16BP in the both mutant strains are comparable (Fig 6). This suggested that in *maf1Δ*, the mechanisms protecting cells from damaging increased concentrations of glycolytic intermediates are unperturbed thus increasing cells survival; cells capable of increased glucose consumption.

Despite the initial rise in F16BP after a glucose pulse, the metabolite attains a steady-state concentration at levels that are not likely to be toxic to the *rpc128-1007* mutant. In *rpc128-1007* cells, we presume that there is no direct relationship between intracellular F16BP and the growth defect on glucose medium exhibited by

bioRxiv preprint doi: https://doi.org/10.1101/372946; this version posted July 20, 2018. The copyright holder for this preprint (which was not certified by peer review) is the author/funder, who has granted bioRxiv a license to display the preprint in perpetuity. It is made available under aCC-BY 4.0 International license.

572 these cells, however alternative scenario is possible, if taking into account the overall abundance of the
573 glycolytic enzymes and an excess of F16BP which may affect Ras proteins. These cells also exhibit large
574 decrease in ribosomal proteins (RP) (S4 Table). RNAP III transcription is coordinately regulated with
575 transcription of rDNA and ribosomal protein coding genes [91,92]. Normally ribosomal proteins and their
576 mRNAs are stabilized when yeast is subject to increased glucose [93]. Arguably, the lower abundance of RP
577 proteins in *rpc128-1007* could reduce the energy expense of cells that are unable to metabolize available
578 extracellular glucose. For the *rpc128-1007*, all of the changes at the proteome level are reminiscent of the
579 global changes in yeast cells in response to environmentally stressful, glucose deprived conditions. An
580 exception is the cohort of proteins of the TCA cycle. RNAP III compromised cells have reduced glycolysis but
581 this reduction does not lead to enhanced oxidative metabolism.
582
583 **_maf1Δ cells_ preferentially metabolizes glucose, which results in carbon overflux fueling the**
584 **side pathways dependent on glycolytic intermediates as precursors.**
585 Lack of Maf1 causes cells to reprogram their metabolism towards higher glycolytic activity when grown under
586 high glucose conditions. This response is not reflected in an increase in abundance of the glycolytic enzymes
587 but rather in enzymatic activity. Of course, the profile of activity modulating posttranslational modifications of
588 these enzymes could well be different in *maf1Δ* but this was beyond the scope of this study. For example,
589 hexokinase 2 exhibited higher activity in *maf1Δ* even though the protein abundance was reduced and the
590 activity of this enzyme is regulated by phosphorylation [94,95]. Higher hexokinase activity should lead to
591 increased flux into glycolysis. However, due to robustness of flux regulation, carbon is redistributed in *maf1Δ*
592 into the side branches of the glycolytic pathway at glucose-6P (Fig 11). The *maf1Δ* shows increased capability
593 to direct carbon into all the side branch pathways as suggested by the proteomic data and confirmed by direct
594 metabolite assay (Fig 7 A). Glucokinase (Glk1), increased in abundance in *maf1Δ,* may redirect glucose toward
595 glycogen storage as previously postulated [96]. The enzymes of glycogen trehalose and central carbon
596 metabolism may be altered in *maf1Δ* as these are dependent on control by the major nutrient sensing protein
597 kinases TOR, PKA, Snf1, Pho85 and the energy sensor Pas kinase [94,97,98].
598

bioRxiv preprint doi: https://doi.org/10.1101/372946; this version posted July 20, 2018. The copyright holder for this preprint (which was not certified by peer review) is the author/funder, who has granted bioRxiv a license to display the preprint in perpetuity. It is made available under aCC-BY 4.0 International license.

In rat hepatoma cells, glucose import, and the activity of hexokinase, hexose phosphate isomerase and the glucose-6P branches that generate F16BP exert most of the flux control [99]. We believe that in *S. cerevisiae*, hexokinase 2 and increased activity of the low affinity glucose transporter Hxt1 have the greatest potential to contribute to flux rerouting in *maf1Δ*. At this stage, we do not know the intracellular signal. The activity of Hxk2 is elevated even though the trehalose shunt, which acts as safety valve against excessive supply of glucose, may correct glucose influx through allosteric inhibition of Hxk2 by trehalose-6P [72,76]. Further the glycolytic flux towards pyruvate could be enhanced by Tdh over-activation. However, carbon flux in *maf1Δ* fuel the glycerol synthesis pathway rather than causing ethanol accumulation. Glycerol accumulation in *maf1Δ* must serve as a drain for excess reducing power, to ameliorate redox imbalance in the cells. *MAF1* deletion in yeast cells is associated with redox imbalance as has previously reported by Bonhoure *et al*. [100] in *MAF1* knock-out mice. In *S. cerevisiae,* this is efficiently counteracted by NADH-consuming glycerol formation [101].

Activation of the branch pathways of the central carbon metabolism seen in *maf1Δ* is a hallmark of cancer cells that reprogram glycolytic activity towards synthesis of metabolites required in excess when cells rapidly divide. For instance, the PP pathway provides precursors for nucleotide and amino acid biosynthesis. This pathway, also referred to as a metabolic redox sensor, is important to maintain carbon homeostasis, is highly correlated to oncogenic, nutrient response signaling pathways [78,102–104] and is required for NADPH regeneration. It supports metabolic reconfiguration in rapidly proliferating cells, since NADPH is a ubiquitous cofactor for most anabolic reductive reactions and got scavenging of reactive oxygen species (ROS) that cause oxidative damage to DNA and proteins and which reduce protein synthesis [105,106]. ROS scavenging enzymes also increased in abundance in *maf1Δ,* suggesting a role of Maf1 in regulation of intracellular redox potential.

How is the glucose flux distributed in Maf1 deficient yeast cells? We propose scenario, build on our observation of the decreased levels of the allosteric activator of pyruvate kinase Cdc19. The reduced F16BP concentration in *maf1Δ* cells could adversely affect Cdc19 activity. The F16BP availability for binding [67–69], but not Cdc19 abundance *per se* or phosphorylation, plays a predominant role in regulating the metabolic flux through the pyruvate kinase Cdc19 [70]. This may further lead to decrease in Cdc19 activity *in vivo* and pushing the glycolytic intermediated of lower glycolysis back to upper side branches of the pathway since lower PEP/pyruvate conversion, catalyzed by pyruvate kinase, favors accumulation of glycolytic intermediates,

bioRxiv preprint doi: https://doi.org/10.1101/372946; this version posted July 20, 2018. The copyright holder for this preprint (which was not certified by peer review) is the author/funder, who has granted bioRxiv a license to display the preprint in perpetuity. It is made available under aCC-BY 4.0 International license.

refueling diverging anabolic pathways, such as the pentose phosphate pathway (PPP) and serine biosynthesis [64,107].

In our model, the glycolytic flux bypasses the steps in upper glycolysis between G6P and G3P, achieved *via* improved flux through PPP. This pathway operates in three modes, depending on a cell demand for metabolic intermediates and cofactors. To avoid extensive F16BP synthesis, which would improve cells survival, the flux should be directed towards glyceraldehydes (G3P) [4]. This scenario is supported by our observation of glycerol accumulation and no change in ethanol production in *maf1Δ* cells. This glucose flux redistribution towards the PPP shunt, amino acids and nucleotide biosynthesis, due to Cdc19 action has been reported for cancer cells [108]. Further, human fibroblasts exposed to hydrogen peroxide elicit enhanced carbon flow through upper glycolysis and the oxidative branch of PPP, causing reduction in lower glycolysis activity [109].

The characteristics of *maf1Δ* in central carbon metabolism is reminiscent of cancer proliferating mammalian cells which are stimulated in the early part of glycolysis *via* PI3K/AKT activation, and making glycolytic intermediates available for macromolecular synthesis due to the low-activity isoform of PK-M2 pyruvate kinase and producing NADPH due to mutated p53 tumor suppressor [107,108].

There are further similarities between *maf1Δ* and mammalian cells after oncogenic transformation. We noted increased potential for amino acid biosynthesis, including the arginine and leucine metabolic pathways. Arg and Leu are crucial for TORC1 signaling and activation of protein translation in yeast and higher eukaryotes. Leucine is the most frequently encoded amino acid in eukaryotic genomes and its levels are sensed by leucyl-tRNA synthetase to activate TORC1 kinase [110,111]. How yeast TORC1 integrates arginine signals is presently unknown. In mammals, arginine levels are communicated by two mechanisms, involving Rag GTPases mediating amino acids signals to control mTORC1 and by a cytoplasmic mechanism that involves arginine signaling by a sensor called CASTOR [112,113].

maf1Δ cells have also a strong enrichment in the branch of serine/cysteine, methionine biosynthesis pathway and in sulfate metabolism by contrast with *rpc128-1007* cells. Methionine biosynthesis is connected to tRNA quality control [114]. A crucial contribution of serine/glycine to cellular metabolism is through the glycine

bioRxiv preprint doi: https://doi.org/10.1101/372946; this version posted July 20, 2018. The copyright holder for this preprint (which was not certified by peer review) is the author/funder, who has granted bioRxiv a license to display the preprint in perpetuity. It is made available under aCC-BY 4.0 International license.

cleavage system, which resupplies once carbon units for one-carbon metabolism The importance of serine/glycine metabolism is emphasized by genetic and functional evidence indicating that hyperactivation of the serine/glycine biosynthetic pathway drives oncogenesis. During growth on a fermentable carbon source, most serine is derived from the phosphoglycerate-3P by the gene products Ser3 and Ser33. Ser3 is a cytosolic enzyme with the dual function of phosphoglycerate dehydrogenase and alpha-ketoglutarate reductase [115]. Known for oxidizing 3-phosphoglycerate in the main serine biosynthesis pathway Ser3 also reduces alpha–ketoglutarate to D-2-hydroxyglutarate (D-2HG) using NADH, the major intracellular source of D-2HG in yeast. High levels of intracellular D-2HG are found in several types of cancer including gliomas and acute myelogenous leukemia [116].

RNAP III genes are not equally regulated by Maf1. Comparison of expression of selected tDNA genes in *maf1Δ* on glucose has revealed elevated $tRNA^{Met}$ levels [13]. Methionine is a proteinogenic amino acid. Over-expression of initiator methionine tRNA ($tRNA^{Met}$) leads to reprogramming of tRNA expression and increased cell metabolic activity in *Drosophila* and proliferation in human epithelial cells [117,118]. Moreover, methionine metabolism influences genomic architecture via H3K4me3 histone methylation to alter chromatin dynamics and cancer associated gene expression [119]. Furthermore, high methionine metabolism and sulfur utilisation is intertwined with high Tkl1 transketolase activity, and is dependent on the non-oxidative phase of the PPP, Tkl1 abundance increased under our study in *maf1Δ* [120]. Methionine biosynthesis, *via* the assimilation of inorganic sulfate, requires three molecules of NADPH per molecule of methionine [80]. The data presented here suggest that efficient supply of NADPH derived from the PPP in *maf1*, may also support methionine biosynthesis in the mutant.

Finally, the proteomics data obtained here with glucose grown *maf1Δ*, suggest an alternative explanation to the reduced fitness of this strain on non-fermentable carbon sources. Down-regulation of *FBP1* transcription (26) is unlikely to be the major cause of *maf1Δ* lethality when grown on glycerol. The *FBP1* gene is expressed only in the absence of glucose, and even if it is not expressed under glucose rich condition that is, under this study the Fbp1 protein is still present in *maf1Δ* at wild-type levels. It is possible that the growth defect in *maf1Δ* on glycerol is due to decrease in abundance of the enzymes involved in the glyoxylate cycle.

bioRxiv preprint doi: https://doi.org/10.1101/372946; this version posted July 20, 2018. The copyright holder for this preprint (which was not certified by peer review) is the author/funder, who has granted bioRxiv a license to display the preprint in perpetuity. It is made available under aCC-BY 4.0 International license.

686 In conclusion, global label-free profiling of enzymatic proteins in yeast has provided new insight in metabolic
687 physiology. Protein abundance patterns characterized in the mutant strains that show different phenotypes on
688 fermentable and non-fermentable carbon source highlighted metabolic pathways that could now be the target
689 for further genetic or metabolic analysis. This work emphasises *S. cerevisiae* as a very good model organism for
690 systems level studies on the dynamics of cellular networks. There is growing evidence for contradictory
691 observations in cultured human cancer cells and in multicellular organisms including mouse models [100,119].
692 We anticipate that yeast cells will continue to be appreciated as a source of basic biological information in
693 building an integrated picture of metabolism and gene regulation.
694

695 ## Conclusions

696 - The capacity of the glycolytic pathway can be altered by manipulation of RNAP III activity.

697 - Lack of Maf1, the negative regulator of RNAP III driven non-coding RNA transcription, enhances glycolytic
698 flux and results in accumulation of end products upstream of pyruvate.

699 - Severe reduction in growth rate caused by RNAP III mutation *rpc128-1007* on glucose is correlated with a
700 decrease in abundance of glycolytic enzymes.

701 - The translation machinery in the *rpc128-1007* mutant seems to be selective towards mRNA coding for
702 enzymes for amino acids synthesis *de novo* at the expense of full complement of glycolytic enzymes.

703 - The critical decrease in abundance of glyoxylate cycle enzymes reduced the ability to convert non-
704 fermentable substrates in *MAF1* knockdown yeast.
705

706 ## Acknowledgments

707 We want to thank Mark Johnston (Dept. of Biochemistry and Molecular Genetics, University of Colorado
708 Denver, US) for providing *pBM2636* plasmid and Emil Furmanek for preparation of samples for proteomics
709 analysis. We are grateful to Dr Philip Brownridge for excellent instrument support. This work was supported by
710 National Science Centre, Poland grant 2012/05/E/NZ2/00583 to M.A. and by funding from Faculty of Chemistry,
711 Warsaw University of Technology, Poland. I dedicate this work to my baby son Piotr.
712

bioRxiv preprint doi: https://doi.org/10.1101/372946; this version posted July 20, 2018. The copyright holder for this preprint (which was not certified by peer review) is the author/funder, who has granted bioRxiv a license to display the preprint in perpetuity. It is made available under aCC-BY 4.0 International license.

713 **Figures captions**

714 **Fig 1. RNAP III regulation by Maf1 and Maf1 interaction network.**

715 A) RNAP III transcription repression is regulated by Maf1. Phosphorylation and dephosphorylation events are
716 involved in the mobility and transportation of Maf1 through the nuclear membrane in which a group of protein
717 kinases are involved in the control of Maf1 nuclear localisation responding to stress events. Maf1 produces
718 transcriptional repression on RNAP III by inducing conformational changes. B) Maf1 protein-protein interaction
719 network. Experimental interactions from STRING database are shown. Nodes have been coloured by protein
720 activity in which different protein complexes related to tRNA modification and transportation can be observed.

721 green: transcription regulation; *MAF1*: negative regulator of RNAP III, *SUB1*: Sub1 transcriptional regulator
722 facilitating elongation through factors that modify RNAP II, role in hyper-osmotic stress response through
723 RANP II and RNAP III, negatively regulates sporulation [121–123], *NOP1*: Nop1, histone glutamine
724 methyltransferase, modifies H2A at Q105 in nucleolus that regulates transcription from the RNAP I promoter
725 involved in C/D snoRNA 3'end processing. Essential gene leads to reduced levels of pre-rRNA species and
726 defects in small ribosomal subunits biogenesis [124–126], *SUA7*: transcriptional factor TFIIB, a general
727 transcription factor required for transcription initiation and start site selection by RNAP II [127,128] - Sub1
728 interaction with TFIIB, [129]. Marine blue: RNAP III holoenzyme subunits, red: protein kinases, *KOG1*: Kog1 the
729 component of the TPR complex, Kog1 depletion display the starvation-like phenotypes- cell growth arrest,
730 reduction in protein synthesis, glycogen accumulation, upregulation in the transcription of nitrogen catabolite
731 repressed and retrograde responses genes conserved in from yeast to man is the homolog of the mammalian
732 TORC1 regulatory protein RAPTOR/mKOG1 [82,130], TOR1 mediates cell growth in response to nutrient
733 availability and cellular stress by regulating protein synthesis, ribosome biogenesis, autophagy, transcription
734 activation cell cycle [131,132] yellow: PKA kinase inhibitor protein *BCY1*, pink: tRNA modification *TAN1*: tRNA
735 modifying proteins Tan1 (responsible for $tRNA^{SER}$ turnover [133]), *TRM1*: Trm1 tRNA methyltranspherase
736 produces modified base N2, n2 dimethylguanosine in tRNA in nucleus and mitochondrion [134], *PUS1*: .*PUS1*
737 associated with human disease [135], introduces pseudouridines in tRNA , also as on *U2* snRNA and
738 pseudouridylation of some mRNA [136,137].),blue: RPC40 (AC40) is a common subunit to RNAP I and III
739 conserve in all eukaryotes [138,139] light blue: *RPO21*: largest subunit of RNAP II, which produces all nuclear

bioRxiv preprint doi: https://doi.org/10.1101/372946; this version posted July 20, 2018. The copyright holder for this preprint (which was not certified by peer review) is the author/funder, who has granted bioRxiv a license to display the preprint in perpetuity. It is made available under aCC-BY 4.0 International license.

740 mRNAs, most snoRNAs and snRNA and the telomerase RNA encoded by *TLC1* [140,141], (according to
741 Saccharomyces Genome Database).

742

743 **Fig 2. Proteome signature of *maf1Δ* and *rpc128-1007* mutants compared to wild-type strain.**
744 A) Histogram of proteins present on both mutants organized according to their corresponding Log_2 fold change
745 expression. B) Comparative scatter plots and histograms of the different strains. The Log_2 transformed protein
746 abundances of proteins present in the WT, *rpc128-1007* and *maf1 Δ* strains are plotted against one another
747 along with their distribution. The number shown is the Pearson correlation coefficient between the two
748 relevant strains. C) Principal component analysis (PCA) based on proteins present on all biological replicates.

749

750 **Fig 3. Increased and decreased protein abundance is presented relative to the wild-type strain for both**
751 ***maf1Δ* and *rpc128-1007* mutants.**
752 All those statically significant proteins with an adjusted *p*-value < 0.05 overlapped between both comparison
753 were then subjected to a hierarchical clustering. This clustering analysis created different groups showing the
754 similarities and differences between both mutants with clusters enriching to biological processes related to
755 amino acid and carbohydrate metabolism, response to stress, and respiratory processes.

756

757 **Fig 4. Comparative proteomic profiling of *maf1Δ* and *rpc128-1007* mutants when compared to wild-type**
758 **strain.**
759 The differences in protein abundances are presented on a schematic representation of the central carbon
760 metabolism. Those proteins with and increased abundance are presented in red and those with an decreased
761 abundance in green.

762

763 **Fig 5. Opposite effects have been observed in *HXT1* promoter activity in strains with altered RNAP III**
764 (A) Schematic representation of glucose uptake and phosphorylation in yeast cells. Hxt – hexose transporter, P
765 – phosphorylation, Hxk1 – hexokinase 1, Hxk2 – hexokinase 2, Glk1 – glucokinase 1. WT, *maf1Δ, rpc128-1007*
766 yeast cells and single or double *HXK1, HXK2, GLK1* knockouts strains in WT, *maf1Δ* and *rpc128-1007* genetic
767 background were cultured in YPD (C) or YPGly (D) rich medium under either inducing (2% glucose) or repressing

bioRxiv preprint doi: https://doi.org/10.1101/372946; this version posted July 20, 2018. The copyright holder for this preprint (which was not certified by peer review) is the author/funder, who has granted bioRxiv a license to display the preprint in perpetuity. It is made available under aCC-BY 4.0 International license.

(2% glycerol) conditions. Maf1 deficiency increases *HXT1* expression (B) on glucose and Hxk2 activity regardless carbon source (C, D). Metabolic effects observed in *rpc128-1007* correlate with decreased *HXT1* expression (B) and decreased hexokinase activity in glucose rich medium (C), but increased hexokinase activity in glycerol rich medium (D). Compromised RNAP III and *maf1Δ* have effect on enzymes in lower glycolysis: Tdh and Cdc19 activities (E and F). The WT strain (MB159-4D), *maf1Δ* and *rpc128-1007* mutant strains were grown under 2% glucose and 2% glycerol conditions. The experiment was performed in cell-free extracts isolated from the aforementioned strains. Data are expressed as the mean obtained from at least three independent experiments measured in triplicate. The + standard deviations are shown. Enzymatic assays were performed in cell-free extracts. The reaction rates were monitored by measuring NADH concentration change over time at 340 nm. V_{max} mean value is expressed as $\mu mol \cdot min^{-1} \cdot mg^{-1}$ protein (C, D, E, F). (B) *HXT1* expression was measured in WT [pBM2636], *maf1Δ* [pBM2636] and *rpc128-1007* [pBM2636] strains by using the *lacZ* reporter gene system [40]. β-galactosidase activity was assayed in cell-free extracts. The error bars indicate the standard deviation from three independent transformants assayed in triplicate. Asterix (*) indicate *p*-value < 0.05 and double asterix (**) illustrate *p*-values < 0.1 according to t-student test.

Fig 6. Changes in intracellular concentration of Fructose 1,6 bisphosphate (F16BP).

Intracellular fructose 1,6 bisphosphate concentration is lowered in cells with changed RNAP III activity under glucose pulse experiment. Cells were grown in YPD until reaching A_{600} ≈ 1.0, collected washed in minimal medium lacking carbon source (CBS-C) and resuspended in CBS (-C). Analysis was performed in a thermostatted vessel at 30°C. Cells were flushed with Ar_2 gas and glucose was added to a final concentration of 2%. Cell samples suspension were collected in time. Fructose 1,6 bisphosphate content was measured by enzymatic breakdown of NADH monitored by changed absorbance at 340 nm in time according to [4]. Fructose 1,6BP concentration was calculated from a standard curve and standardized to cells dry weight expressed in g. Results are shown as mean value for four biological replicates.

Fig 7. Maf1 deficient yeast strain accumulates glycogen (A) and trehalose (B) during exponential phase.

Yeast were cultivated in rich medium supplemented with 2% glucose and harvested by centrifugation at A_{600} ≈ 1.0. Glucose concentration from enzymatic breakdown of glycogen (A) by amyloglucosidase from *A. niger,* was determined by Glucose (HK) Assay Kit (GAHK-20, Sigma). Trehalose (B) content determination assay was

bioRxiv preprint doi: https://doi.org/10.1101/372946; this version posted July 20, 2018. The copyright holder for this preprint (which was not certified by peer review) is the author/funder, who has granted bioRxiv a license to display the preprint in perpetuity. It is made available under aCC-BY 4.0 International license.

797 performed using Trehalose Assay Kit (Megazyme) according to manufacturer's protocol. Trehalose and
798 glycogen content is presentment as mean value of at least three independent biological replicates with
799 standard deviations. There were no significant changes in ethanol production rate between wild-type (MB159-
800 4D) and *maf1Δ* strain (C). *maf1Δ* accumulated glycerol (D). Ethanol and glycerol concentration was determined
801 under Fermentative capacity assay (FCA) conditions in *maf1Δ* strain (C and D). Fermentative capacity assay was
802 performed as described by van Hoek *et al.* (1998) [49] with modifications (for details see Method section). All
803 assays were performed in triplicates. Results are shown as mean concentration [g/L] value with standard
804 deviation in time [min]. 'C-limited' stands for 'carbon-limited conditions'. Asterix (*) indicate *p*-value < 0.05 and
805 double asterix (**) illustrate *p*-values < 0.1 according to t-student test.
806
807 **Fig 8. Amino acid biosynthesis and associated proteome signature.**
808 Abundance protein patterns for amino acid metabolism are presented showing those proteins with and
809 increased abundance in red and those with an decreased abundance in green.
810
811 **Fig 9. *GCN4* transcripts and Gcn4 protein relative levels are significantly increased *rpc128-1007* yeast cells**
812 **and moderately in *maf1Δ* cells.**
813 Yeast cells were grown in rich medium supplemented with 2% glucose until reached exponential growth phase
814 (A_{600} ≈ 1.0). SYBER-Green based Real-Time PCR (A) showed that *GCN4* transcript increased 2-fold in *maf1Δ* and
815 by 11-fold in *rpc128-1007*. Wild-type strain expression level was taken as 1.0. Samples were normalized to two
816 reference genes - *U2* spliceosomal RNA (*U2*) and small cytosolic RNA (*SCR1*). Asterisk (*) indicates *p*-values
817 lowered than 0.05 according to t-student test. Western blotting assay (B) showed increased stability of Gcn4-
818 3HA protein in *maf1Δ* and *rpc128-1007* mutant strains expressing chromosomally encoded Gcn4-3HA. Total cell
819 protein extracts were subjected to SDS-PAGE and examined by Western blotting with anti-HA antibodies (B).
820 Quantitative relative level of Gcn4–3HA protein in comparison to yeast Vma2 protein level was calculated for at
821 least three independent biological replicates (C).
822
823 **Fig 10. Transcription factor enrichment analysis.**
824 Enrichment in the proteome sets for individual transcription factors was calculated using the GeneCodis
825 website taking the sets of proteins with an adjusted *p*-value of < 0.05 from both strains *maf1Δ* and *rpc128-1007*

bioRxiv preprint doi: https://doi.org/10.1101/372946; this version posted July 20, 2018. The copyright holder for this preprint (which was not certified by peer review) is the author/funder, who has granted bioRxiv a license to display the preprint in perpetuity. It is made available under aCC-BY 4.0 International license.

826 compared against the wild-type. Proteins were classified according to their positive or negative fold change and
827 the background set consisted of all proteins identified in the given MS experiment.
828
829 **Fig 11. Proposed model of carbon flow in *rpc128-1007* and *maf1Δ* yeast cells**.
830 Altered RNAP III activity affects carbon flux. Low activity of RNAP III in *rpc128-1007* strain is correlated with
831 decreased carbon flow through glycolysis in comparison to reference strain. By contrast, *maf1Δ* cells
832 demonstrate increased carbon flow through hexokinase step and lower glycolysis compared to the control
833 strain. In *maf1Δ*, excess glucose-6-P (G6P) is redirected into PPP and trehalose and glycogen biosynthesis. As a
834 result fructose 1,6 bisphosphate (F16BP) concentration decreases in *maf1Δ*. From the increased glycerol
835 concentration, carbon flux is partially redirected towards upper glycolysis at PEP. Green: decrease in carbon
836 flux; Red: increase in carbon flux. Legend: glucose-6-phosphate (G6P); fructose-6-phosphate (F6P); fructose 1,6
837 bisphosphate (F16BP); dihydroxyacetone phosphate (DHAP); glyceraldehyde-3-phosphate (G3P); 6-
838 phosphogluconate (6PG); ribose 5-phosphate (R5P); 3-phosphoglyceric acid (3PG); phosphoenolpyruvate (PEP).
839
840
841

bioRxiv preprint doi: https://doi.org/10.1101/372946; this version posted July 20, 2018. The copyright holder for this preprint (which was not certified by peer review) is the author/funder, who has granted bioRxiv a license to display the preprint in perpetuity. It is made available under aCC-BY 4.0 International license.

842 ## References

843 1. Otterstedt K, Larsson C, Bill RM, Ståhlberg A, Boles E, Hohmann S, et al. Switching the mode of
844 metabolism in the yeast Saccharomyces cerevisiae. EMBO Rep. 2004 May;5(5):532–7.

845 2. Dechant R, Binda M, Lee SS, Pelet S, Winderickx J, Peter M. Cytosolic pH is a second messenger for
846 glucose and regulates the PKA pathway through V-ATPase. EMBO J. 2010 Aug 4;29(15):2515–26.

847 3. Zhang C-S, Hawley SA, Zong Y, Li M, Wang Z, Gray A, et al. Fructose-1,6-bisphosphate and aldolase
848 mediate glucose sensing by AMPK. Nature. 2017 Aug 3;548(7665):112–6.

849 4. Peeters K, Van FL, Fischer B, Bonini BM, Quezada H, Tsytlonok M, et al. Fructose-1,6-bisphosphate
850 couples glycolytic flux to activation of Ras., Fructose-1,6-bisphosphate couples glycolytic flux to activation of
851 Ras. Nat Commun. 2017;8, 8(1):922–922.

852 5. Mitchison JM. The Biology of the Cell Cycle. CUP Archive; 1971. 324 p.

853 6. Elliott SG, McLaughlin CS. Rate of macromolecular synthesis through the cell cycle of the yeast
854 Saccharomyces cerevisiae. Proc Natl Acad Sci U S A. 1978 Sep;75(9):4384–8.

855 7. Polymenis M, Aramayo R. Translate to divide: control of the cell cycle by protein synthesis. Microb
856 Cell. 2015 Mar 20;2(4):94–104.

857 8. Waldron C. Synthesis of Ribosomal and Transfer Ribonucleic Acids in Yeast During a Nutritional Shift-
858 up. Journal of General Microbiology. 1977 Jan 1;98(1):215–21.

859 9. Kief DR, Warner JR. Coordinate control of syntheses of ribosomal ribonucleic acid and ribosomal
860 proteins during nutritional shift-up in Saccharomyces cerevisiae. Molecular and Cellular Biology. 1981
861 Nov;1(11):1007–15.

862 10. Boguta M, Czerska K, Zoładek T. Mutation in a new gene MAF1 affects tRNA suppressor efficiency in
863 Saccharomyces cerevisiae. Gene. 1997 Feb 7;185(2):291–6.

864 11. Pluta K, Lefebvre O, Martin NC, Smagowicz WJ, Stanford DR, Ellis SR, et al. Maf1p, a Negative Effector
865 of RNA Polymerase III in Saccharomyces cerevisiae. Mol Cell Biol. 2001 Aug;21(15):5031–40.

866 12. Upadhya R, Lee J, Willis IM. Maf1 Is an Essential Mediator of Diverse Signals that Repress RNA
867 Polymerase III Transcription. Molecular Cell. 2002 Dec;10(6):1489–94.

868 13. Cieśla M, Towpik J, Graczyk D, Oficjalska-Pham D, Harismendy O, Suleau A, et al. Maf1 Is Involved in
869 Coupling Carbon Metabolism to RNA Polymerase III Transcription. Mol Cell Biol. 2007 Nov;27(21):7693–702.

bioRxiv preprint doi: https://doi.org/10.1101/372946; this version posted July 20, 2018. The copyright holder for this preprint (which was not certified by peer review) is the author/funder, who has granted bioRxiv a license to display the preprint in perpetuity. It is made available under aCC-BY 4.0 International license.

14. Vannini A, Ringel R, Kusser AG, Berninghausen O, Kassavetis GA, Cramer P. Molecular Basis of RNA Polymerase III Transcription Repression by Maf1. Cell. 2010 Oct;143(1):59–70.

15. Oficjalska-Pham D, Harismendy O, Smagowicz WJ, Gonzalez de Peredo A, Boguta M, Sentenac A, et al. General repression of RNA polymerase III transcription is triggered by protein phosphatase type 2A-mediated dephosphorylation of Maf1. Mol Cell. 2006 Jun 9;22(5):623–32.

16. Zaragoza O, Gancedo JM. Elements from the cAMP signaling pathway are involved in the control of expression of the yeast gluconeogenic gene FBP1. FEBS Lett. 2001 Oct 12;506(3):262–6.

17. Harismendy O, Gendrel C-G, Soularue P, Gidrol X, Sentenac A, Werner M, et al. Genome-wide location of yeast RNA polymerase III transcription machinery. EMBO J. 2003 Sep 15;22(18):4738–47.

18. Reina JH, Azzouz TN, Hernandez N. Maf1, a New Player in the Regulation of Human RNA Polymerase III Transcription. PLOS ONE. 2006 Dec 27;1(1):e134.

19. Desai N, Lee J, Upadhya R, Chu Y, Moir RD, Willis IM. Two Steps in Maf1-dependent Repression of Transcription by RNA Polymerase III. J Biol Chem. 2005 Feb 25;280(8):6455–62.

20. Moir RD, Lee J, Haeusler RA, Desai N, Engelke DR, Willis IM. Protein kinase A regulates RNA polymerase III transcription through the nuclear localization of Maf1. Proc Natl Acad Sci USA. 2006 Oct 10;103(41):15044–9.

21. Roberts DN, Wilson B, Huff JT, Stewart AJ, Cairns BR. Dephosphorylation and genome-wide association of Maf1 with Pol III-transcribed genes during repression. Mol Cell. 2006 Jun 9;22(5):633–44.

22. Boisnard S, Lagniel G, Garmendia-Torres C, Molin M, Boy-Marcotte E, Jacquet M, et al. H2O2 activates the nuclear localization of Msn2 and Maf1 through thioredoxins in Saccharomyces cerevisiae. Eukaryotic Cell. 2009 Sep;8(9):1429–38.

23. Lee J, Moir RD, Willis IM. Regulation of RNA Polymerase III Transcription Involves SCH9-dependent and SCH9-independent Branches of the Target of Rapamycin (TOR) Pathway. J Biol Chem. 2009 May 8;284(19):12604–8.

24. Wei Y, Tsang CK, Zheng XFS. Mechanisms of regulation of RNA polymerase III-dependent transcription by TORC1. EMBO J. 2009 Aug 5;28(15):2220–30.

25. Graczyk D, Debski J, Muszyńska G, Bretner M, Lefebvre O, Boguta M. Casein kinase II-mediated phosphorylation of general repressor Maf1 triggers RNA polymerase III activation. Proc Natl Acad Sci USA. 2011 Mar 22;108(12):4926–31.

bioRxiv preprint doi: https://doi.org/10.1101/372946; this version posted July 20, 2018. The copyright holder for this preprint (which was not certified by peer review) is the author/funder, who has granted bioRxiv a license to display the preprint in perpetuity. It is made available under aCC-BY 4.0 International license.

898 26. Morawiec E, Wichtowska D, Graczyk D, Conesa C, Lefebvre O, Boguta M. Maf1, repressor of tRNA
899 transcription, is involved in the control of gluconeogenetic genes in Saccharomyces cerevisiae. Gene. 2013
900 Aug;526(1):16–22.
901 27. Adamczyk M, Szatkowska R. Low RNA Polymerase III activity results in up regulation of HXT2 glucose
902 transporter independently of glucose signaling and despite changing environment. PLOS ONE. 2017 Sep
903 29;12(9):e0185516.
904 28. Kwapisz M, Smagowicz WJ, Oficjalska D, Hatin I, Rousset J-P, Żołądek T, et al. Up-regulation of tRNA
905 biosynthesis affects translational readthrough in maf1-Δ mutant of Saccharomyces cerevisiae. Curr Genet. 2002
906 Dec 1;42(3):147–52.
907 29. Longtine MS, Mckenzie III A, Demarini DJ, Shah NG, Wach A, Brachat A, et al. Additional modules for
908 versatile and economical PCR-based gene deletion and modification in Saccharomyces cerevisiae. Yeast. 1998
909 Jul 1;14(10):953–61.
910 30. Gietz RD, Schiestl RH. Large-scale high-efficiency yeast transformation using the LiAc/SS carrier
911 DNA/PEG method. Nat Protocols. 2007 Jan;2(1):38–41.
912 31. Bradford MM. A rapid and sensitive method for the quantitation of microgram quantities of protein
913 utilizing the principle of protein-dye binding. Analytical Biochemistry. 1976 May;72(1):248–54.
914 32. Cox J, Mann M. MaxQuant enables high peptide identification rates, individualized p.p.b.-range mass
915 accuracies and proteome-wide protein quantification. Nat Biotech. 2008 Dec;26(12):1367–72.
916 33. Choi M, Chang C-Y, Clough T, Broudy D, Killeen T, MacLean B, et al. MSstats: an R package for
917 statistical analysis of quantitative mass spectrometry-based proteomic experiments. Bioinformatics. 2014 Sep
918 1;30(17):2524–6.
919 34. Mi H, Muruganujan A, Thomas PD. PANTHER in 2013: modeling the evolution of gene function, and
920 other gene attributes, in the context of phylogenetic trees. Nucleic Acids Res. 2013 Jan;41(Database
921 issue):D377–86.
922 35. Kanehisa M, Furumichi M, Tanabe M, Sato Y, Morishima K. KEGG: new perspectives on genomes,
923 pathways, diseases and drugs. Nucleic Acids Res. 2017 Jan 4;45(Database issue):D353–61.
924 36. Jensen LJ, Kuhn M, Stark M, Chaffron S, Creevey C, Muller J, et al. STRING 8—a global view on proteins
925 and their functional interactions in 630 organisms. Nucleic Acids Res. 2009 Jan;37(Database issue):D412–6.

bioRxiv preprint doi: https://doi.org/10.1101/372946; this version posted July 20, 2018. The copyright holder for this preprint (which was not certified by peer review) is the author/funder, who has granted bioRxiv a license to display the preprint in perpetuity. It is made available under aCC-BY 4.0 International license.

926 37. Shannon P, Markiel A, Ozier O, Baliga NS, Wang JT, Ramage D, et al. Cytoscape: A Software
927 Environment for Integrated Models of Biomolecular Interaction Networks. Genome Res. 2003 Nov
928 1;13(11):2498–504.
929 38. Carmona-Saez P, Chagoyen M, Tirado F, Carazo JM, Pascual-Montano A. GENECODIS: a web-based tool
930 for finding significant concurrent annotations in gene lists. Genome Biol. 2007;8(1):R3.
931 39. Cankorur-Cetinkaya A, Dereli E, Eraslan S, Karabekmez E, Dikicioglu D, Kirdar B. A Novel Strategy for
932 Selection and Validation of Reference Genes in Dynamic Multidimensional Experimental Design in Yeast. PLoS
933 One. 2012 Jun 4;7(6).
934 40. Ozcan S, Johnston M. Three different regulatory mechanisms enable yeast hexose transporter (HXT)
935 genes to be induced by different levels of glucose. Mol Cell Biol. 1995 Mar;15(3):1564–72.
936 41. Adamczyk M, van Eunen K, Bakker BM, Westerhoff HV. Enzyme Kinetics for Systems Biology. Methods
937 in Enzymology. 2011 Jan 1;500:233–57.
938 42. De Winde JH, Crauwels M, Hohmann S, Thevelein JM, Winderickx J. Differential requirement of the
939 yeast sugar kinases for sugar sensing in establishing the catabolite-repressed state. Eur J Biochem. 1996 Oct
940 15;241(2):633–43.
941 43. Grüning N-M, Rinnerthaler M, Bluemlein K, Mülleder M, Wamelink MMC, Lehrach H, et al. Pyruvate
942 Kinase Triggers a Metabolic Feedback Loop that Controls Redox Metabolism in Respiring Cells. Cell Metab. 2011
943 Sep 7;14(3):415–27.
944 44. Postma E, Verduyn C, Scheffers WA, Dijken JPV. Enzymic analysis of the crabtree effect in glucose-
945 limited chemostat cultures of Saccharomyces cerevisiae. Applied and Environmental Microbiology. 1989
946 Feb;55(2):468.
947 45. Smale ST. Beta-galactosidase assay. Cold Spring Harb Protoc. 2010 May;2010(5):pdb.prot5423.
948 46. Beers RF, Sizer IW. A spectrophotometric method for measuring the breakdown of hydrogen peroxide
949 by catalase. J Biol Chem. 1952 Mar;195(1):133–40.
950 47. Rossouw D, Heyns EH, Setati ME, Bosch S, Bauer FF. Adjustment of Trehalose Metabolism in Wine
951 Saccharomyces cerevisiae Strains To Modify Ethanol Yields. Appl Environ Microbiol. 2013 Sep 1;79(17):5197–
952 207.
953 48. Parrou JL, François J. A Simplified Procedure for a Rapid and Reliable Assay of both Glycogen and
954 Trehalose in Whole Yeast Cells. Analytical Biochemistry. 1997 May 15;248(1):186–8.

bioRxiv preprint doi: https://doi.org/10.1101/372946; this version posted July 20, 2018. The copyright holder for this preprint (which was not certified by peer review) is the author/funder, who has granted bioRxiv a license to display the preprint in perpetuity. It is made available under aCC-BY 4.0 International license.

955 49. Van Hoek P, Van Dijken JP, Pronk JT. Effect of Specific Growth Rate on Fermentative Capacity of
956 Baker's Yeast. Appl Environ Microbiol. 1998 Nov;64(11):4226–33.
957 50. Picotti P, Bodenmiller B, Mueller LN, Domon B, Aebersold R. Full dynamic range proteome analysis of
958 S. cerevisiae by targeted proteomics. Cell. 2009 Aug 21;138(4):795–806.
959 51. Feng Y, De Franceschi G, Kahraman A, Soste M, Melnik A, Boersema PJ, et al. Global analysis of protein
960 structural changes in complex proteomes. Nat Biotechnol. 2014 Oct;32(10):1036–44.
961 52. Carlson M. Glucose repression in yeast. Current Opinion in Microbiology. 1999 Apr 1;2(2):202–7.
962 53. Young ET, Dombek KM, Tachibana C, Ideker T. Multiple Pathways Are Co-regulated by the Protein
963 Kinase Snf1 and the Transcription Factors Adr1 and Cat8. J Biol Chem. 2003 Jul 11;278(28):26146–58.
964 54. Wendell DL, Bisson LF. Expression of high-affinity glucose transport protein Hxt2p of Saccharomyces
965 cerevisiae is both repressed and induced by glucose and appears to be regulated posttranslationally. J
966 Bacteriol. 1994 Jun;176(12):3730–7.
967 55. Galazzo JL, Bailey JE. Growing Saccharomyces cerevisiae in calcium-alginate beads induces cell
968 alterations which accelerate glucose conversion to ethanol. Biotechnology and Bioengineering. 1990 Aug
969 5;36(4):417–26.
970 56. Rolland F, Winderickx J, Thevelein JM. Glucose-sensing and -signalling mechanisms in yeast. FEMS
971 Yeast Research. 2002 May;2(2):183–201.
972 57. Elbing K, Larsson C, Bill RM, Albers E, Snoep JL, Boles E, et al. Role of hexose transport in control of
973 glycolytic flux in Saccharomyces cerevisiae. Appl Environ Microbiol. 2004 Sep;70(9):5323–30.
974 58. Guillaume C, Delobel P, Sablayrolles J-M, Blondin B. Molecular Basis of Fructose Utilization by the Wine
975 Yeast Saccharomyces cerevisiae: a Mutated HXT3 Allele Enhances Fructose Fermentation. Appl Environ
976 Microbiol. 2007 Apr;73(8):2432–9.
977 59. Lane S, Xu H, Oh EJ, Kim H, Lesmana A, Jeong D, et al. Glucose repression can be alleviated by reducing
978 glucose phosphorylation rate in Saccharomyces cerevisiae. Scientific Reports. 2018 Feb 8;8(1):2613.
979 60. Herrero P, Galíndez J, Ruiz N, Martínez-Campa C, Moreno F. Transcriptional regulation of the
980 Saccharomyces cerevisiae HXK1, HXK2 and GLK1 genes. Yeast. 1995 Feb;11(2):137–44.
981 61. Bakker BM, Walsh MC, ter Kuile BH, Mensonides FIC, Michels PAM, Opperdoes FR, et al. Contribution
982 of glucose transport to the control of the glycolytic flux in Trypanosoma brucei. Proc Natl Acad Sci U S A. 1999
983 Aug 31;96(18):10098–103.

bioRxiv preprint doi: https://doi.org/10.1101/372946; this version posted July 20, 2018. The copyright holder for this preprint (which was not certified by peer review) is the author/funder, who has granted bioRxiv a license to display the preprint in perpetuity. It is made available under aCC-BY 4.0 International license.

984 62. Shestov AA, Liu X, Ser Z, Cluntun AA, Hung YP, Huang L, et al. Quantitative determinants of aerobic
985 glycolysis identify flux through the enzyme GAPDH as a limiting step. Elife. 2014 Jul 9;3.
986 63. Pearce AK, Crimmins K, Groussac E, Hewlins MJE, Dickinson JR, Francois J, et al. Pyruvate kinase (Pyk1)
987 levels influence both the rate and direction of carbon flux in yeast under fermentative conditions.
988 Microbiology. 2001;147(2):391–401.
989 64. Zampar GG, Kümmel A, Ewald J, Jol S, Niebel B, Picotti P, et al. Temporal system-level organization of
990 the switch from glycolytic to gluconeogenic operation in yeast. Mol Syst Biol. 2013 Apr 2;9:651.
991 65. Zheng L, Roeder RG, Luo Y. S Phase Activation of the Histone H2B Promoter by OCA-S, a Coactivator
992 Complex that Contains GAPDH as a Key Component. Cell. 2003 Jul 25;114(2):255–66.
993 66. White MR, Garcin ED. The sweet side of RNA regulation: glyceraldehyde-3-phosphate dehydrogenase
994 as a noncanonical RNA-binding protein. Wiley Interdiscip Rev RNA. 2016;7(1):53–70.
995 67. Blair JB, Walker RG. Rat liver pyruvate kinase: influence of ligands on activity and fructose 1,6-
996 bisphosphate binding. Arch Biochem Biophys. 1984 Jul;232(1):202–13.
997 68. Jurica MS, Mesecar A, Heath PJ, Shi W, Nowak T, Stoddard BL. The allosteric regulation of pyruvate
998 kinase by fructose-1,6-bisphosphate. Structure. 1998 Feb 15;6(2):195–210.
999 69. Dombrauckas JD, Santarsiero BD, Mesecar AD. Structural basis for tumor pyruvate kinase M2 allosteric
1000 regulation and catalysis. Biochemistry. 2005 Jul 12;44(27):9417–29.
1001 70. Xu Y-F, Zhao X, Glass DS, Absalan F, Perlman DH, Broach JR, et al. Regulation of yeast pyruvate kinase
1002 by ultrasensitive allostery independent of phosphorylation. Mol Cell. 2012 Oct 12;48(1):52–62.
1003 71. Apweiler E, Sameith K, Margaritis T, Brabers N, van de Pasch L, Bakker LV, et al. Yeast glucose
1004 pathways converge on the transcriptional regulation of trehalose biosynthesis. BMC Genomics. 2012 Jun
1005 14;13:239.
1006 72. Hohmann S, Bell W, NevesA MJ, Valckx D, Thevelein JM. Evidence for trehalose-6-phosphate-
1007 dependent and -independent mechanisms in the control of sugar influx into yeast glycolysis. Molecular
1008 Microbiology. 1996 Jun 1;20(5):981–91.
1009 73. Teusink B, Walsh MC, van Dam K, Westerhoff HV. The danger of metabolic pathways with turbo
1010 design. Trends Biochem Sci. 1998 May;23(5):162–9.
1011 74. Heerden JH van, Wortel MT, Bruggeman FJ, Heijnen JJ, Bollen YJM, Planqué R, et al. Lost in Transition:
1012 Start-Up of Glycolysis Yields Subpopulations of Nongrowing Cells. Science. 2014 Feb 28;343(6174):1245114.

bioRxiv preprint doi: https://doi.org/10.1101/372946; this version posted July 20, 2018. The copyright holder for this preprint (which was not certified by peer review) is the author/funder, who has granted bioRxiv a license to display the preprint in perpetuity. It is made available under aCC-BY 4.0 International license.

1013 75. Shulman RG, Rothman DL. Homeostasis and the glycogen shunt explains aerobic ethanol production in
1014 yeast. PNAS. 2015 Sep 1;112(35):10902–7.
1015 76. Blázquez MA, Lagunas R, Gancedo C, Gancedo JM. Trehalose-6-phosphate, a new regulator of yeast
1016 glycolysis that inhibits hexokinases. FEBS Letters. 1993 Aug;329(1):51–4.
1017 77. Gancedo C, Flores C-L. The importance of a functional trehalose biosynthetic pathway for the life of
1018 yeasts and fungi. FEMS Yeast Res. 2004 Jan;4(4–5):351–9.
1019 78. Krüger A, Grüning N-M, Wamelink MMC, Kerick M, Kirpy A, Parkhomchuk D, et al. The pentose
1020 phosphate pathway is a metabolic redox sensor and regulates transcription during the antioxidant response.
1021 Antioxid Redox Signal. 2011 Jul 15;15(2):311–24.
1022 79. Stanton RC. Glucose-6-Phosphate Dehydrogenase, NADPH, and Cell Survival. IUBMB Life. 2012
1023 May;64(5):362–9.
1024 80. Stincone A, Prigione A, Cramer T, Wamelink MMC, Campbell K, Cheung E, et al. The return of
1025 metabolism: biochemistry and physiology of the pentose phosphate pathway. Biol Rev Camb Philos Soc. 2015
1026 Aug;90(3):927–63.
1027 81. Hinnebusch AG. Translational regulation of GCN4 and the general amino acid control of yeast. Annu
1028 Rev Microbiol. 2005;59:407–50.
1029 82. Loewith R, Hall MN. Target of Rapamycin (TOR) in Nutrient Signaling and Growth Control. Genetics.
1030 2011 Dec;189(4):1177–201.
1031 83. Natarajan K, Meyer MR, Jackson BM, Slade D, Roberts C, Hinnebusch AG, et al. Transcriptional profiling
1032 shows that Gcn4p is a master regulator of gene expression during amino acid starvation in yeast. Mol Cell Biol.
1033 2001 Jul;21(13):4347–68.
1034 84. Conesa C, Ruotolo R, Soularue P, Simms TA, Donze D, Sentenac A, et al. Modulation of yeast genome
1035 expression in response to defective RNA polymerase III-dependent transcription. Mol Cell Biol. 2005
1036 Oct;25(19):8631–42.
1037 85. Chou H-J, Donnard E, Gustafsson HT, Garber M, Rando OJ. Transcriptome-wide Analysis of Roles for
1038 tRNA Modifications in Translational Regulation. Mol Cell. 2017 Dec 7;68(5):978-992.e4.
1039 86. Vilela C, Linz B, Rodrigues-Pousada C, McCarthy JE. The yeast transcription factor genes YAP1 and YAP2
1040 are subject to differential control at the levels of both translation and mRNA stability. Nucleic Acids Res. 1998
1041 Mar 1;26(5):1150–9.

bioRxiv preprint doi: https://doi.org/10.1101/372946; this version posted July 20, 2018. The copyright holder for this preprint (which was not certified by peer review) is the author/funder, who has granted bioRxiv a license to display the preprint in perpetuity. It is made available under aCC-BY 4.0 International license.

87. Filer D, Thompson MA, Takhaveev V, Dobson AJ, Kotronaki I, Green JWM, et al. RNA polymerase III limits longevity downstream of TORC1. Nature. 2017 Dec 14;552(7684):263–7.

88. Mannhaupt G, Schnall R, Karpov V, Vetter I, Feldmann H. Rpn4p acts as a transcription factor by binding to PACE, a nonamer box found upstream of 26S proteasomal and other genes in yeast. FEBS Lett. 1999 Apr 30;450(1–2):27–34.

89. Xie Y, Varshavsky A. RPN4 is a ligand, substrate, and transcriptional regulator of the 26S proteasome: a negative feedback circuit. Proc Natl Acad Sci USA. 2001 Mar 13;98(6):3056–61.

90. Harding HP, Novoa I, Zhang Y, Zeng H, Wek R, Schapira M, et al. Regulated translation initiation controls stress-induced gene expression in mammalian cells. Mol Cell. 2000 Nov;6(5):1099–108.

91. Li Y, Moir RD, Sethy-Coraci IK, Warner JR, Willis IM. Repression of Ribosome and tRNA Synthesis in Secretion-Defective Cells Is Signaled by a Novel Branch of the Cell Integrity Pathway. Mol Cell Biol. 2000 Jun;20(11):3843–51.

92. Upadhya R, Lee J, Willis IM. Maf1 is an essential mediator of diverse signals that repress RNA polymerase III transcription. Mol Cell. 2002 Dec;10(6):1489–94.

93. Yin Z, Wilson S, Hauser NC, Tournu H, Hoheisel JD, Brown AJP. Glucose triggers different global responses in yeast, depending on the strength of the signal, and transiently stabilizes ribosomal protein mRNAs. Mol Microbiol. 2003 May;48(3):713–24.

94. Oliveira AP, Ludwig C, Picotti P, Kogadeeva M, Aebersold R, Sauer U. Regulation of yeast central metabolism by enzyme phosphorylation. Mol Syst Biol. 2012 Nov 13;8:623.

95. Barbosa AD, Pereira C, Osório H, Moradas-Ferreira P, Costa V. The ceramide-activated protein phosphatase Sit4p controls lifespan, mitochondrial function and cell cycle progression by regulating hexokinase 2 phosphorylation. Cell Cycle. 2016 May 10;15(12):1620–30.

96. Ihmels JH, Bergmann S. Challenges and prospects in the analysis of large-scale gene expression data. Brief Bioinformatics. 2004 Dec;5(4):313–27.

97. François J, Parrou JL. Reserve carbohydrates metabolism in the yeast Saccharomyces cerevisiae. FEMS Microbiology Reviews. 2001 Jan;25(1):125–45.

98. Ptacek J, Devgan G, Michaud G, Zhu H, Zhu X, Fasolo J, et al. Global analysis of protein phosphorylation in yeast. Nature. 2005 Dec;438(7068):679–84.

bioRxiv preprint doi: https://doi.org/10.1101/372946; this version posted July 20, 2018. The copyright holder for this preprint (which was not certified by peer review) is the author/funder, who has granted bioRxiv a license to display the preprint in perpetuity. It is made available under aCC-BY 4.0 International license.

1070 99. Marín-Hernández A, Rodríguez-Enríquez S, Vital-González PA, Flores-Rodríguez FL, Macías-Silva M,
1071 Sosa-Garrocho M, et al. Determining and understanding the control of glycolysis in fast-growth tumor cells.
1072 Flux control by an over-expressed but strongly product-inhibited hexokinase. FEBS J. 2006 May;273(9):1975–
1073 88.
1074 100. Bonhoure N, Byrnes A, Moir RD, Hodroj W, Preitner F, Praz V, et al. Loss of the RNA polymerase III
1075 repressor MAF1 confers obesity resistance. Genes Dev. 2015 May 1;29(9):934–47.
1076 101. van Dijken JP, van den Bosch E, Hermans JJ, de Miranda LR, Scheffers WA. Alcoholic fermentation by
1077 'non-fermentative' yeasts. Yeast. 1986 Jun;2(2):123–7.
1078 102. Godon C, Lagniel G, Lee J, Buhler JM, Kieffer S, Perrot M, et al. The H2O2 stimulon in Saccharomyces
1079 cerevisiae. J Biol Chem. 1998 Aug 28;273(35):22480–9.
1080 103. Ralser M, Wamelink MM, Kowald A, Gerisch B, Heeren G, Struys EA, et al. Dynamic rerouting of the
1081 carbohydrate flux is key to counteracting oxidative stress. J Biol. 2007 Dec 21;6(4):10.
1082 104. Patra KC, Hay N. The pentose phosphate pathway and cancer. Trends Biochem Sci. 2014
1083 Aug;39(8):347–54.
1084 105. Delaunay A, Pflieger D, Barrault MB, Vinh J, Toledano MB. A thiol peroxidase is an H2O2 receptor and
1085 redox-transducer in gene activation. Cell. 2002 Nov 15;111(4):471–81.
1086 106. Shenton D, Grant CM. Protein S-thiolation targets glycolysis and protein synthesis in response to
1087 oxidative stress in the yeast Saccharomyces cerevisiae. Biochem J. 2003 Sep 1;374(Pt 2):513–9.
1088 107. Amelio I, Cutruzzolá F, Antonov A, Agostini M, Melino G. Serine and glycine metabolism in cancer.
1089 Trends Biochem Sci. 2014 Apr;39(4):191–8.
1090 108. Heiden MGV, Cantley LC, Thompson CB. Understanding the Warburg Effect: The Metabolic
1091 Requirements of Cell Proliferation. Science. 2009 May 22;324(5930):1029–33.
1092 109. Kuehne A, Emmert H, Soehle J, Winnefeld M, Fischer F, Wenck H, et al. Acute Activation of Oxidative
1093 Pentose Phosphate Pathway as First-Line Response to Oxidative Stress in Human Skin Cells. Molecular Cell.
1094 2015 Aug 6;59(3):359–71.
1095 110. Echols N, Harrison P, Balasubramanian S, Luscombe NM, Bertone P, Zhang Z, et al. Comprehensive
1096 analysis of amino acid and nucleotide composition in eukaryotic genomes, comparing genes and pseudogenes.
1097 Nucleic Acids Res. 2002 Jun 1;30(11):2515–23.

bioRxiv preprint doi: https://doi.org/10.1101/372946; this version posted July 20, 2018. The copyright holder for this preprint (which was not certified by peer review) is the author/funder, who has granted bioRxiv a license to display the preprint in perpetuity. It is made available under aCC-BY 4.0 International license.

111. Avruch J, Long X, Ortiz-Vega S, Rapley J, Papageorgiou A, Dai N. Amino acid regulation of TOR complex 1. Am J Physiol Endocrinol Metab. 2009 Apr;296(4):E592-602.

112. Sancak Y, Peterson TR, Shaul YD, Lindquist RA, Thoreen CC, Bar-Peled L, et al. The Rag GTPases bind raptor and mediate amino acid signaling to mTORC1. Science. 2008 Jun 13;320(5882):1496–501.

113. Saxton RA, Chantranupong L, Knockenhauer KE, Schwartz TU, Sabatini DM. Mechanism of arginine sensing by CASTOR1 upstream of mTORC1. Nature. 2016 11;536(7615):229–33.

114. Hopper AK. Transfer RNA Post-Transcriptional Processing, Turnover, and Subcellular Dynamics in the Yeast Saccharomyces cerevisiae. Genetics. 2013 May;194(1):43–67.

115. Becker-Kettern J, Paczia N, Conrotte J-F, Kay DP, Guignard C, Jung PP, et al. Saccharomyces cerevisiae Forms D-2-Hydroxyglutarate and Couples Its Degradation to D-Lactate Formation via a Cytosolic Transhydrogenase. J Biol Chem. 2016 Mar 18;291(12):6036–58.

116. Losman J-A, Kaelin WG. What a difference a hydroxyl makes: mutant IDH, (R)-2-hydroxyglutarate, and cancer. Genes Dev. 2013 Apr 15;27(8):836–52.

117. Rideout EJ, Marshall L, Grewal SS. Drosophila RNA polymerase III repressor Maf1 controls body size and developmental timing by modulating tRNAiMet synthesis and systemic insulin signaling. Proc Natl Acad Sci USA. 2012 Jan 24;109(4):1139–44.

118. Pavon-Eternod M, Gomes S, Rosner MR, Pan T. Overexpression of initiator methionine tRNA leads to global reprogramming of tRNA expression and increased proliferation in human epithelial cells. RNA. 2013 Apr;19(4):461–6.

119. Dai Z, Mentch SJ, Gao X, Nichenametla SN, Locasale JW. Methionine metabolism influences genomic architecture and gene expression through H3K4me3 peak width. Nat Commun. 2018 May 16;9.

120. Campbell K, Vowinckel J, Keller MA, Ralser M. Methionine Metabolism Alters Oxidative Stress Resistance via the Pentose Phosphate Pathway. Antioxid Redox Signal. 2016 Apr 1;24(10):543–7.

121. Knaus R, Pollock R, Guarente L. Yeast SUB1 is a suppressor of TFIIB mutations and has homology to the human co-activator PC4. EMBO J. 1996 Apr 15;15(8):1933–40.

122. Calvo O, Manley JL. The transcriptional coactivator PC4/Sub1 has multiple functions in RNA polymerase II transcription. EMBO J. 2005 Mar 9;24(5):1009–20.

123. Rosonina E, Willis IM, Manley JL. Sub1 functions in osmoregulation and in transcription by both RNA polymerases II and III. Mol Cell Biol. 2009 Apr;29(8):2308–21.

bioRxiv preprint doi: https://doi.org/10.1101/372946; this version posted July 20, 2018. The copyright holder for this preprint (which was not certified by peer review) is the author/funder, who has granted bioRxiv a license to display the preprint in perpetuity. It is made available under aCC-BY 4.0 International license.

124. Henríquez R, Blobel G, Aris JP. Isolation and sequencing of NOP1. A yeast gene encoding a nucleolar protein homologous to a human autoimmune antigen. J Biol Chem. 1990 Feb 5;265(4):2209–15.

125. Schimmang T, Tollervey D, Kern H, Frank R, Hurt EC. A yeast nucleolar protein related to mammalian fibrillarin is associated with small nucleolar RNA and is essential for viability. EMBO J. 1989 Dec 20;8(13):4015–24.

126. Tessarz P, Santos-Rosa H, Robson SC, Sylvestersen KB, Nelson CJ, Nielsen ML, et al. Glutamine methylation in histone H2A is an RNA-polymerase-I-dedicated modification. Nature. 2014 Jan 23;505(7484):564–8.

127. Pinto I, Ware DE, Hampsey M. The yeast SUA7 gene encodes a homolog of human transcription factor TFIIB and is required for normal start site selection in vivo. Cell. 1992 Mar 6;68(5):977–88.

128. Wu WH, Pinto I, Chen BS, Hampsey M. Mutational analysis of yeast TFIIB. A functional relationship between Ssu72 and Sub1/Tsp1 defined by allele-specific interactions with TFIIB. Genetics. 1999 Oct;153(2):643–52.

129. Cho EJ, Buratowski S. Evidence that transcription factor IIB is required for a post-assembly step in transcription initiation. J Biol Chem. 1999 Sep 3;274(36):25807–13.

130. Kim D-H, Sarbassov DD, Ali SM, King JE, Latek RR, Erdjument-Bromage H, et al. mTOR interacts with raptor to form a nutrient-sensitive complex that signals to the cell growth machinery. Cell. 2002 Jul 26;110(2):163–75.

131. Inoki K, Ouyang H, Li Y, Guan K-L. Signaling by target of rapamycin proteins in cell growth control. Microbiol Mol Biol Rev. 2005 Mar;69(1):79–100.

132. Martin DE, Hall MN. The expanding TOR signaling network. Curr Opin Cell Biol. 2005 Apr;17(2):158–66.

133. Turowski TW, Karkusiewicz I, Kowal J, Boguta M. Maf1-mediated repression of RNA polymerase III transcription inhibits tRNA degradation via RTD pathway. RNA. 2012 Oct;18(10):1823–32.

134. Ellis SR, Morales MJ, Li JM, Hopper AK, Martin NC. Isolation and characterization of the TRM1 locus, a gene essential for the N2,N2-dimethylguanosine modification of both mitochondrial and cytoplasmic tRNA in Saccharomyces cerevisiae. J Biol Chem. 1986 Jul 25;261(21):9703–9.

135. Powell CA, Nicholls TJ, Minczuk M. Nuclear-encoded factors involved in post-transcriptional processing and modification of mitochondrial tRNAs in human disease. Front Genet. 2015;6:79.

bioRxiv preprint doi: https://doi.org/10.1101/372946; this version posted July 20, 2018. The copyright holder for this preprint (which was not certified by peer review) is the author/funder, who has granted bioRxiv a license to display the preprint in perpetuity. It is made available under aCC-BY 4.0 International license.

136. Massenet S, Motorin Y, Lafontaine DL, Hurt EC, Grosjean H, Branlant C. Pseudouridine mapping in the Saccharomyces cerevisiae spliceosomal U small nuclear RNAs (snRNAs) reveals that pseudouridine synthase pus1p exhibits a dual substrate specificity for U2 snRNA and tRNA. Mol Cell Biol. 1999 Mar;19(3):2142–54.

137. Carlile TM, Rojas-Duran MF, Zinshteyn B, Shin H, Bartoli KM, Gilbert WV. Pseudouridine profiling reveals regulated mRNA pseudouridylation in yeast and human cells. Nature. 2014 Nov 6;515(7525):143–6.

138. Lalo D, Carles C, Sentenac A, Thuriaux P. Interactions between three common subunits of yeast RNA polymerases I and III. Proc Natl Acad Sci USA. 1993 Jun 15;90(12):5524–8.

139. Huang Y, Maraia RJ. Comparison of the RNA polymerase III transcription machinery in Schizosaccharomyces pombe, Saccharomyces cerevisiae and human. Nucleic Acids Res. 2001 Jul 1;29(13):2675–90.

140. Cramer P, Bushnell DA, Fu J, Gnatt AL, Maier-Davis B, Thompson NE, et al. Architecture of RNA polymerase II and implications for the transcription mechanism. Science. 2000 Apr 28;288(5466):640–9.

141. Chapon C, Cech TR, Zaug AJ. Polyadenylation of telomerase RNA in budding yeast. RNA. 1997 Nov;3(11):1337–51.

bioRxiv preprint doi: https://doi.org/10.1101/372946; this version posted July 20, 2018. The copyright holder for this preprint (which was not certified by peer review) is the author/funder, who has granted bioRxiv a license to display the preprint in perpetuity. It is made available under aCC-BY 4.0 International license.

Supporting information

S1 Fig. Zwf1 (A) and the Ctt1 catalase activity (B) is increased in Maf1 deficient mutant.

Yeast cells logarithmically growing in YPD 2% glucose medium were harvested at A_{600} ≈ 1.0. For Zwf1 activity assay, NADH breakdown was measured at 340 nm in time at 30°C. For catalase activity, hydrogen peroxide decomposition in reaction mixtures containing yeast cell free extracts was monitored as change in absorbance at 240 nm in time at 30°C. Results are presented as total mean enzymatic activity from five independent biological replicates with standard deviation expressed as $\mu mol \cdot min^{-1} \cdot mg^{-1}$ protein. Asterix (*) indicate *p*-value < 0.05 according to t-student test.

S2 Fig. Real-time quantitative PCR analyses of *LEU3* gene transcript.

Slight increase in *LEU3* transcript levels was observed in *rpc128-1007* in glucose medium. Opposite effect was observed on glycerol-based rich medium. Maf1 deficiency cause 2-fold decrease in *LEU3* mRNA levels, when grown non-fermentative carbon source and reduced in glucose-based rich medium. Yeast cells were grown in 2% glucose (YPD) or 2% glycerol (YPGly) rich medium at 30°C until an A_{600} ≈ 1.0. SYBER-Green based Real-Time PCR was performed. The expression level of each target PCR product was normalized to reference genes transcript levels: *U2* spliceosomal RNA (*U2*) and small cytosolic RNA (*SCR1)*. The means + standard deviations of the relative expression levels from three independent biological replicates are shown. The value of basal gene expression level of WT strain was assumed as 1.0. Asterisks (*) indicate *p*-values ≤ 0.05 determined by t-student test.

S1 Table. Mean value for triplicate experiments of fermentative capacity assay of WT and *maf1Δ* cells. Results are expressed in mM / g dry weight. 'C-limited' stands for 'carbon-limited conditions'.

S2 Table. The list of 8 proteins involved in oxidative stress with higher abundance in *maf1Δ* and lowered quantity in *rpc128-1007* mutant in comparison to wild-type reference strain under high glucose conditions according to global proteomics.

bioRxiv preprint doi: https://doi.org/10.1101/372946; this version posted July 20, 2018. The copyright holder for this preprint (which was not certified by peer review) is the author/funder, who has granted bioRxiv a license to display the preprint in perpetuity. It is made available under aCC-BY 4.0 International license.

S3 Table. The list of 18 proteins regulated by RPN4 that are part of 26S proteasome and its core complex, 20S proteasome, with lowered abundance in *rpc128-1007* mutant in comparison to wild-type reference strain under high glucose conditions according to global proteomics.

S4 Table. The list of 73 proteins involved in ribosome biogenesis with lowered abundance in *rpc128-1007* mutant in comparison to wild-type reference strain under high glucose conditions according to global proteomics.

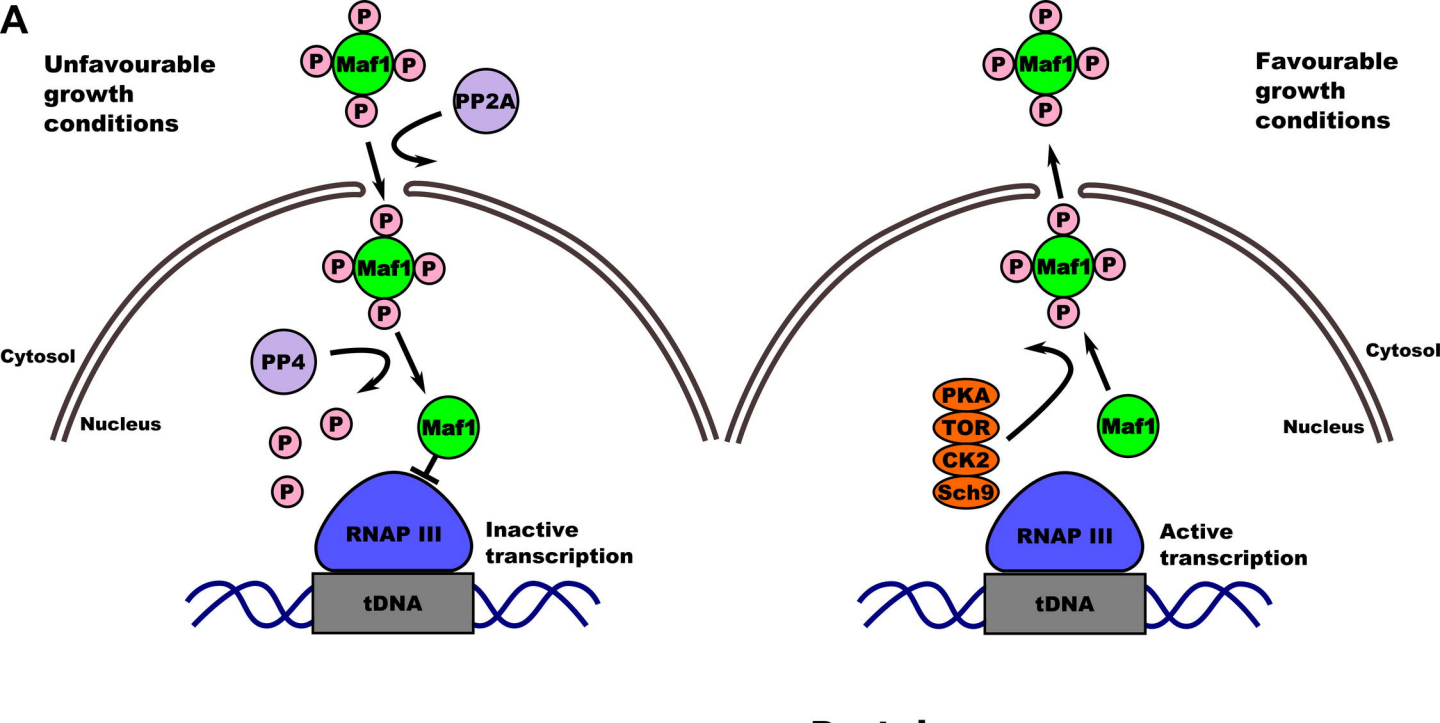
A
Unfavourable growth conditions
Favourable growth conditions
Maf1
PP2A
PP4
Cytosol
Nucleus
RNAP III
tDNA
Inactive transcription
Active transcription
PKA
TOR
CK2
Sch9

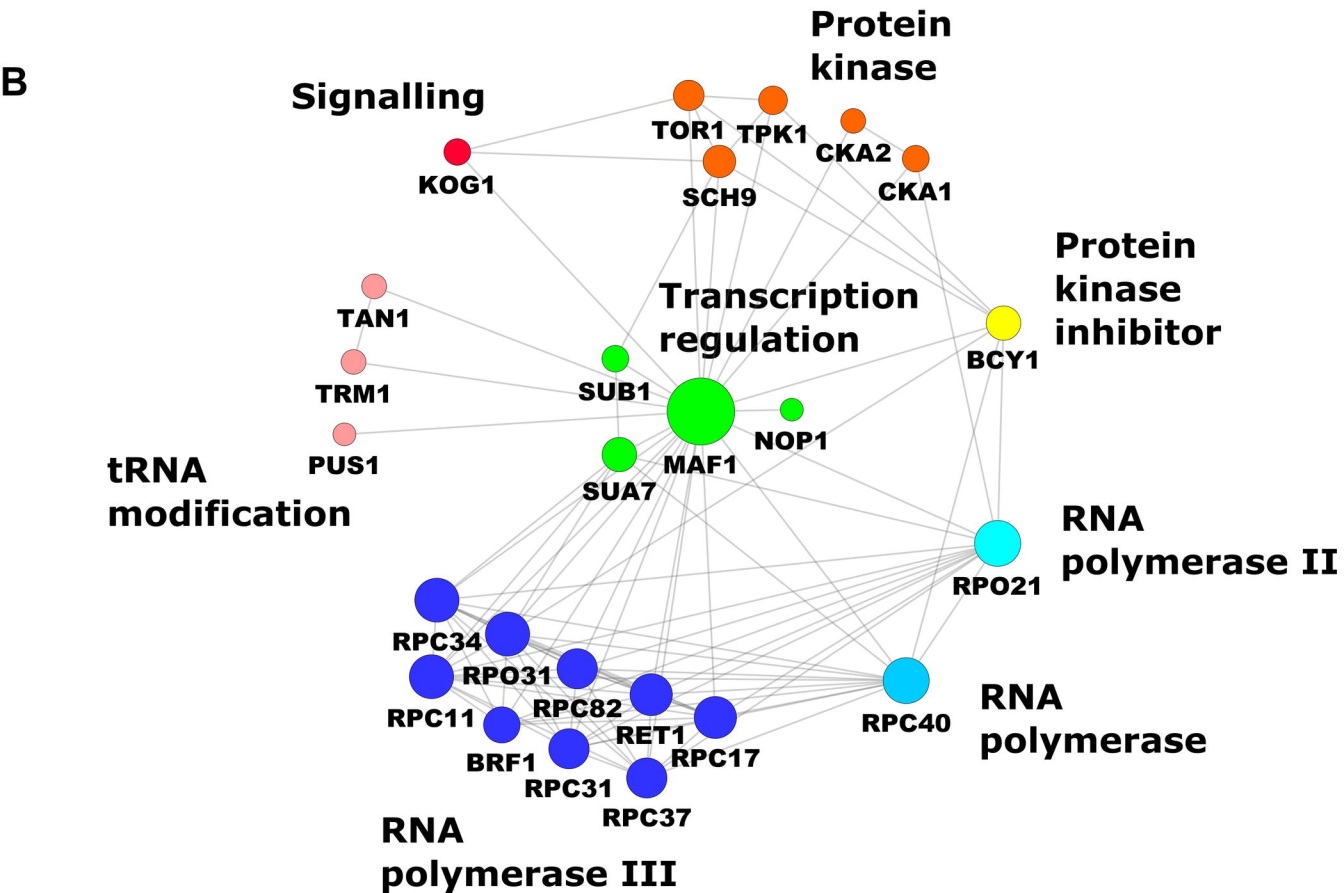
B
Protein kinase
Signalling
TOR1
TPK1
CKA2
CKA1
KOG1
SCH9
Protein kinase inhibitor
Transcription regulation
TAN1
TRM1
PUS1
SUB1
NOP1
MAF1
SUA7
BCY1
tRNA modification
RNA polymerase II
RPO21
RPC34
RPO31
RPC11
RPC82
RET1
RPC17
BRF1
RPC31
RPC37
RPC40
RNA polymerase
RNA polymerase III

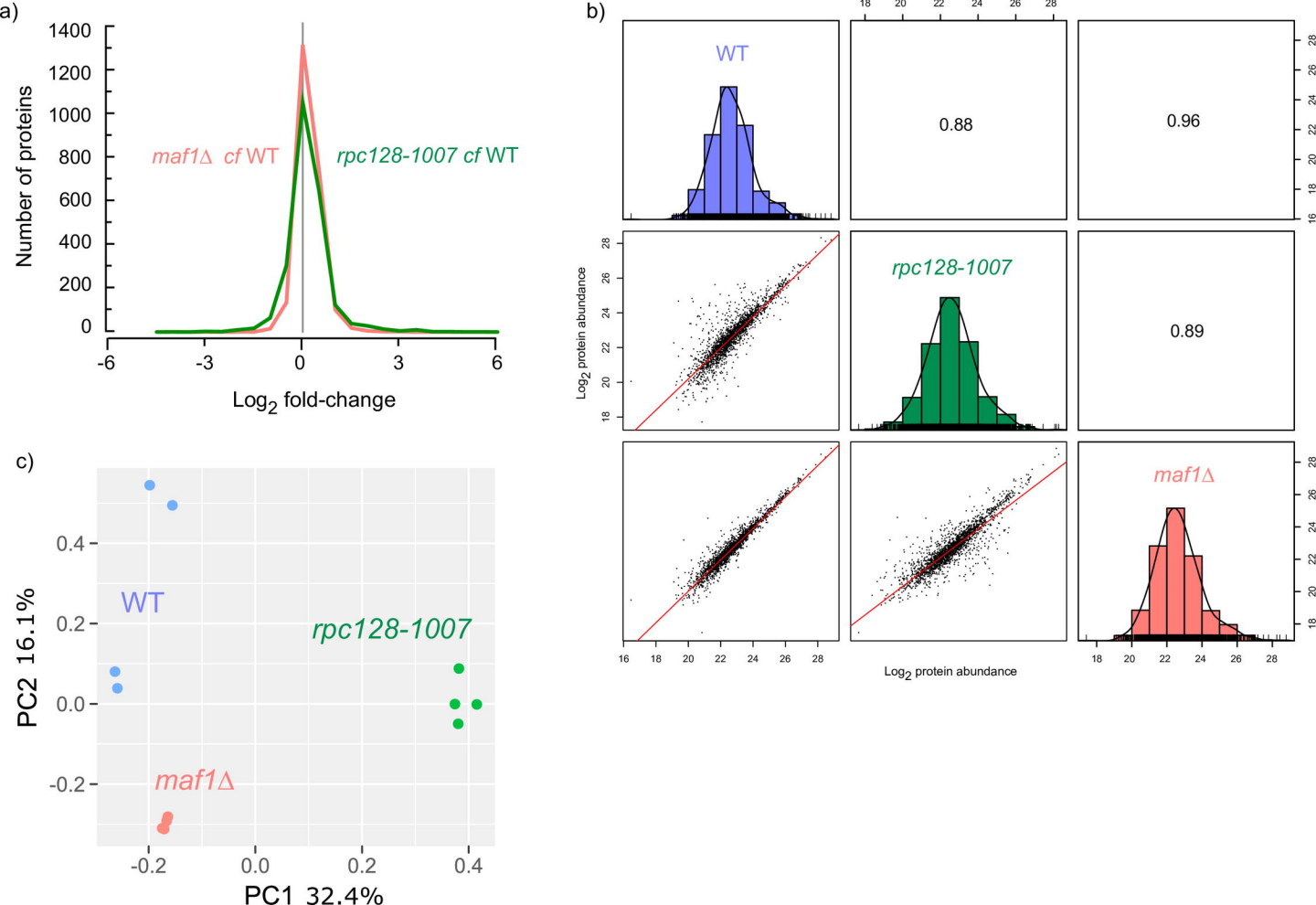
a)
Number of proteins
1400
1200
1000
800
600
400
200
0
maf1Δ cf WT
rpc128-1007 cf WT
-6
-3
0
3
6
Log2 fold-change
b)
WT
0.88
0.96
rpc128-1007
0.89
maf1Δ
Log2 protein abundance
Log2 protein abundance
c)
WT
rpc128-1007
maf1Δ
PC2 16.1%
PC1 32.4%
0.4
0.2
0.0
-0.2
-0.2
0.0
0.2
0.4

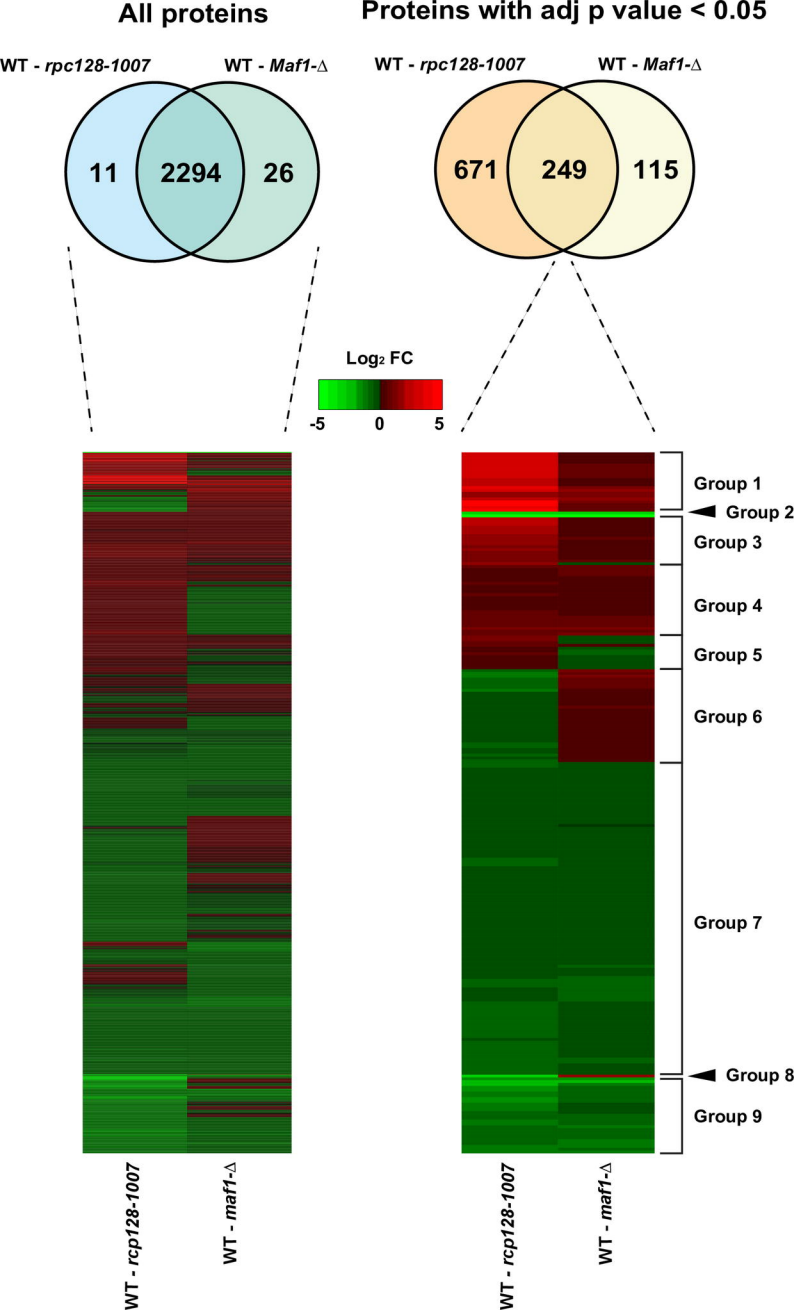

	Enriched GO biological process
Group 1	Arginine biosynthetic process Ornithine biosynthetic process Urea cycle Leucine biosynthetic process Aspartate family amino acid biosynthetic process
Group 2	Glyoxylate cycle Gluconeogenesis
Group 3	Aromatic amino acid family biosynthetic process Lysine biosynthetic process Tryptophan metabolic process Methionine biosynthetic process Dicarboxylic acid metabolic process
Group 4	Homocysteine metabolic process Carboxylic acid biosynthetic process
Group 5	Glycine catabolic process Cellular amino acid metabolic process
Group 6	Trehalose metabolism in response to stress Trehalose biosynthetic process Replicative cell aging Cellular response to oxidative stress Single-organism carbohydrate catabolic process Response to oxygen-containint compound Oxidation-reduction process
Group 7	Chaperone-mediated protein folding 'De novo' protein folding Purine ribonucleoside monophosphate biosynthetic process Purine ribonucleotide biosynthetic process Mitochondrial transmembrane transport Cytoplasmic translation Single-organism intracellular transport Cellular macromolecular complex assembly
Group 8	Alcohol dehydrogenase
Group 9	'De novo' IMP biosynthetic process Tricarboxylic acid cycle Carbohydrate metabolic process

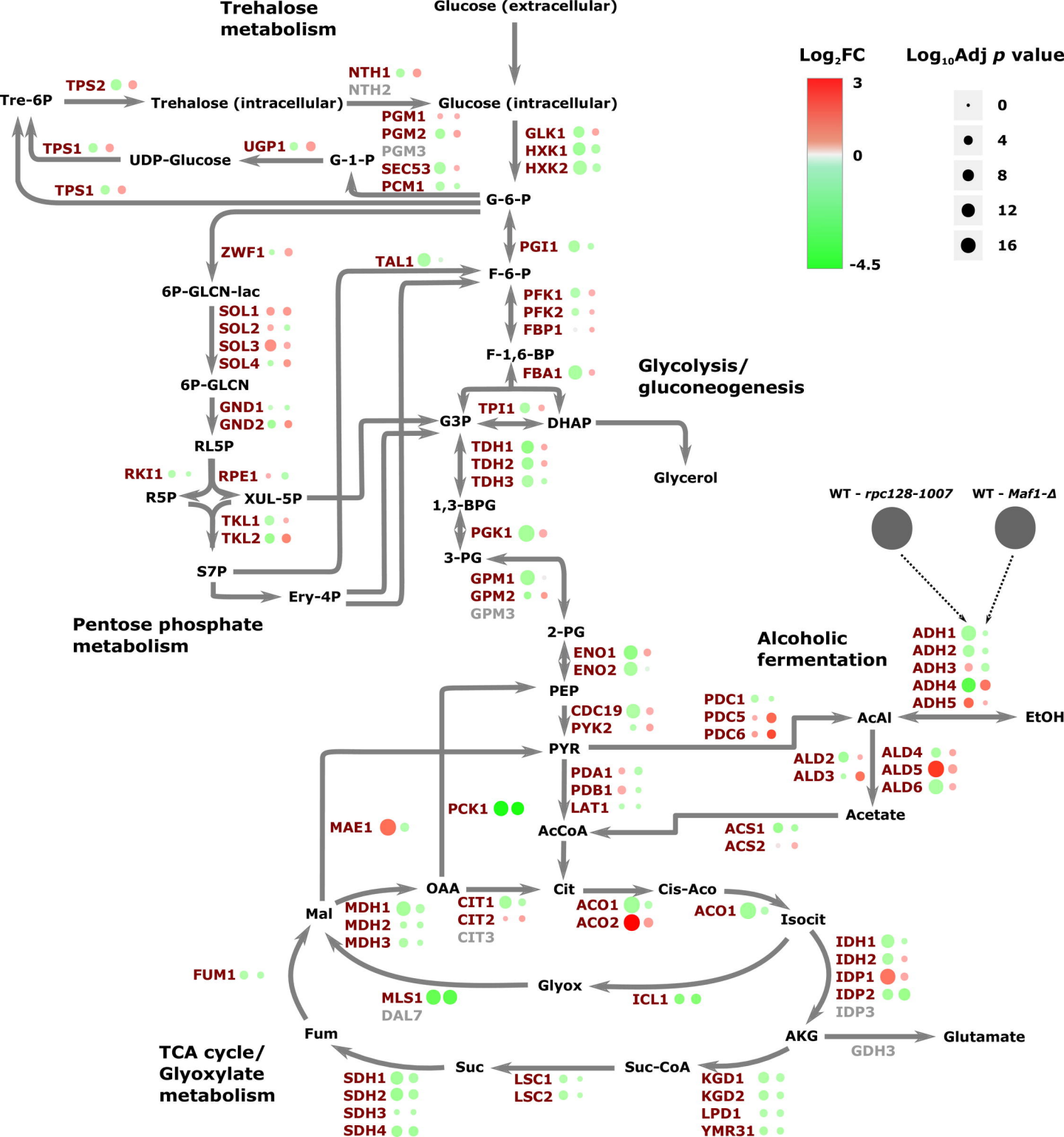
Trehalose metabolism
Glucose (extracellular)
Log2FC
3
0
-4.5
Log10Adj p value
0
4
8
12
16
TPS2
Tre-6P
Trehalose (intracellular)
NTH1
NTH2
Glucose (intracellular)
PGM1
PGM2
PGM3
SEC53
PCM1
GLK1
HXK1
HXK2
TPS1
UDP-Glucose
UGP1
G-1-P
TPS1
G-6-P
ZWF1
PGI1
TAL1
F-6-P
6P-GLCN-lac
PFK1
PFK2
FBP1
SOL1
SOL2
SOL3
SOL4
F-1,6-BP
FBA1
Glycolysis/ gluconeogenesis
6P-GLCN
GND1
GND2
TPI1
G3P
DHAP
RL5P
TDH1
TDH2
TDH3
Glycerol
RKI1
RPE1
R5P
XUL-5P
1,3-BPG
TKL1
TKL2
PGK1
3-PG
S7P
GPM1
GPM2
GPM3
Ery-4P
Pentose phosphate metabolism
2-PG
ENO1
ENO2
PEP
CDC19
PYK2
PDC1
PDC5
PDC6
AcAl
EtOH
PYR
ALD2
ALD3
ALD4
ALD5
ALD6
PDA1
PDB1
LAT1
PCK1
Acetate
MAE1
AcCoA
ACS1
ACS2
OAA
Cit
Cis-Aco
Mal
MDH1
MDH2
MDH3
CIT1
CIT2
CIT3
ACO1
ACO2
ACO1
Isocit
IDH1
IDH2
IDP1
IDP2
IDP3
FUM1
Glyox
MLS1
DAL7
ICL1
Fum
AKG
Glutamate
GDH3
TCA cycle/ Glyoxylate metabolism
Suc
Suc-CoA
SDH1
SDH2
SDH3
SDH4
LSC1
LSC2
KGD1
KGD2
LPD1
YMR31
WT - rpc128-1007
WT - Maf1-Δ
Alcoholic fermentation
ADH1
ADH2
ADH3
ADH4
ADH5

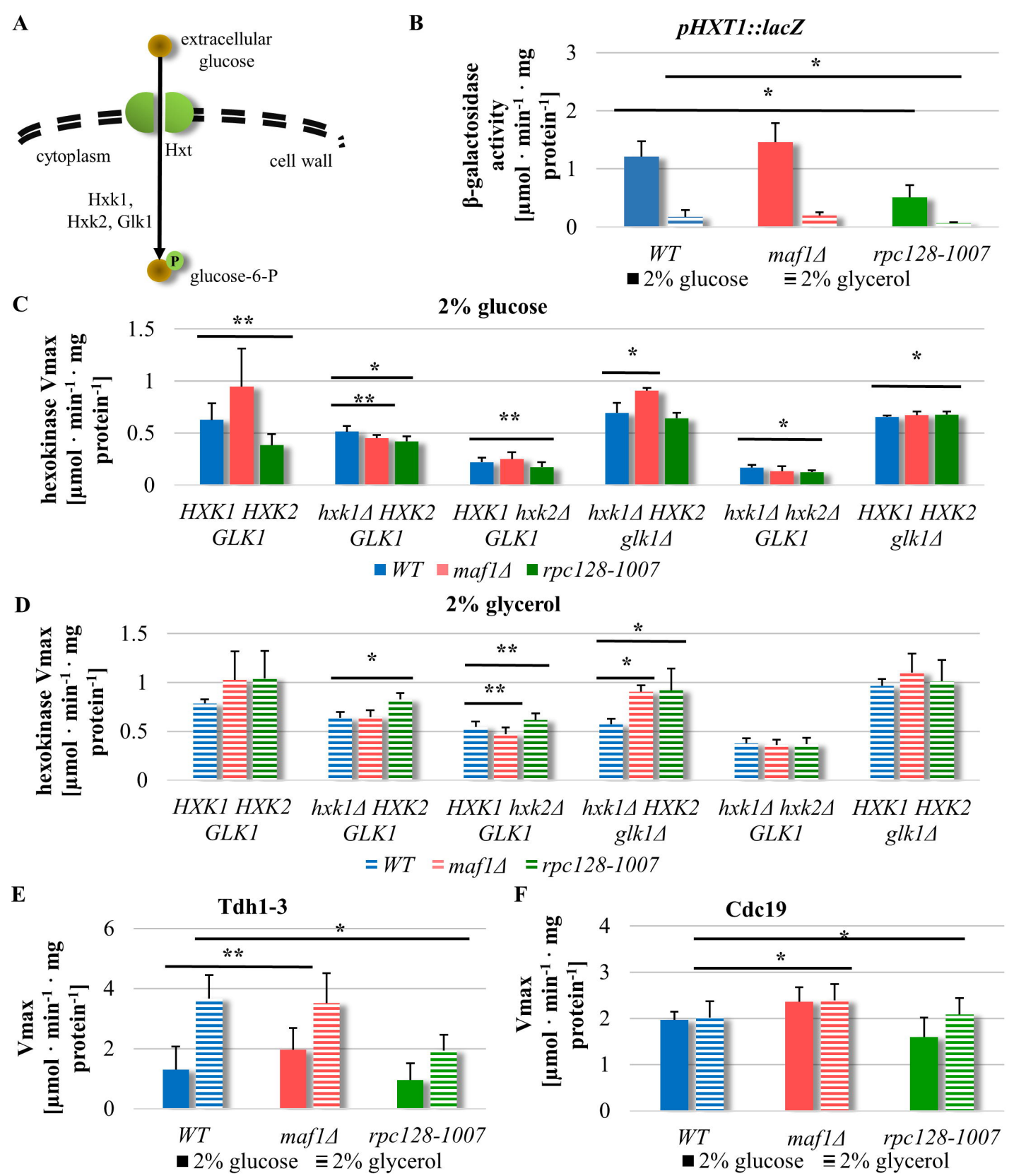
A
extracellular glucose
cytoplasm
Hxt
cell wall
Hxk1, Hxk2, Glk1
P
glucose-6-P
B
pHXT1::lacZ
β-galactosidase activity [μmol · min-1 · mg protein-1]
WT
maf1Δ
rpc128-1007
2% glucose
2% glycerol
C
2% glucose
hexokinase Vmax [μmol · min-1 · mg protein-1]
HXK1 HXK2 GLK1
hxk1Δ HXK2 GLK1
HXK1 hxk2Δ GLK1
hxk1Δ HXK2 glk1Δ
hxk1Δ hxk2Δ GLK1
HXK1 HXK2 glk1Δ
WT
maf1Δ
rpc128-1007
D
2% glycerol
hexokinase Vmax [μmol · min-1 · mg protein-1]
HXK1 HXK2 GLK1
hxk1Δ HXK2 GLK1
HXK1 hxk2Δ GLK1
hxk1Δ HXK2 glk1Δ
hxk1Δ hxk2Δ GLK1
HXK1 HXK2 glk1Δ
WT
maf1Δ
rpc128-1007
E
Tdh1-3
Vmax [μmol · min-1 · mg protein-1]
WT
maf1Δ
rpc128-1007
2% glucose
2% glycerol
F
Cdc19
Vmax [μmol · min-1 · mg protein-1]
WT
maf1Δ
rpc128-1007
2% glucose
2% glycerol

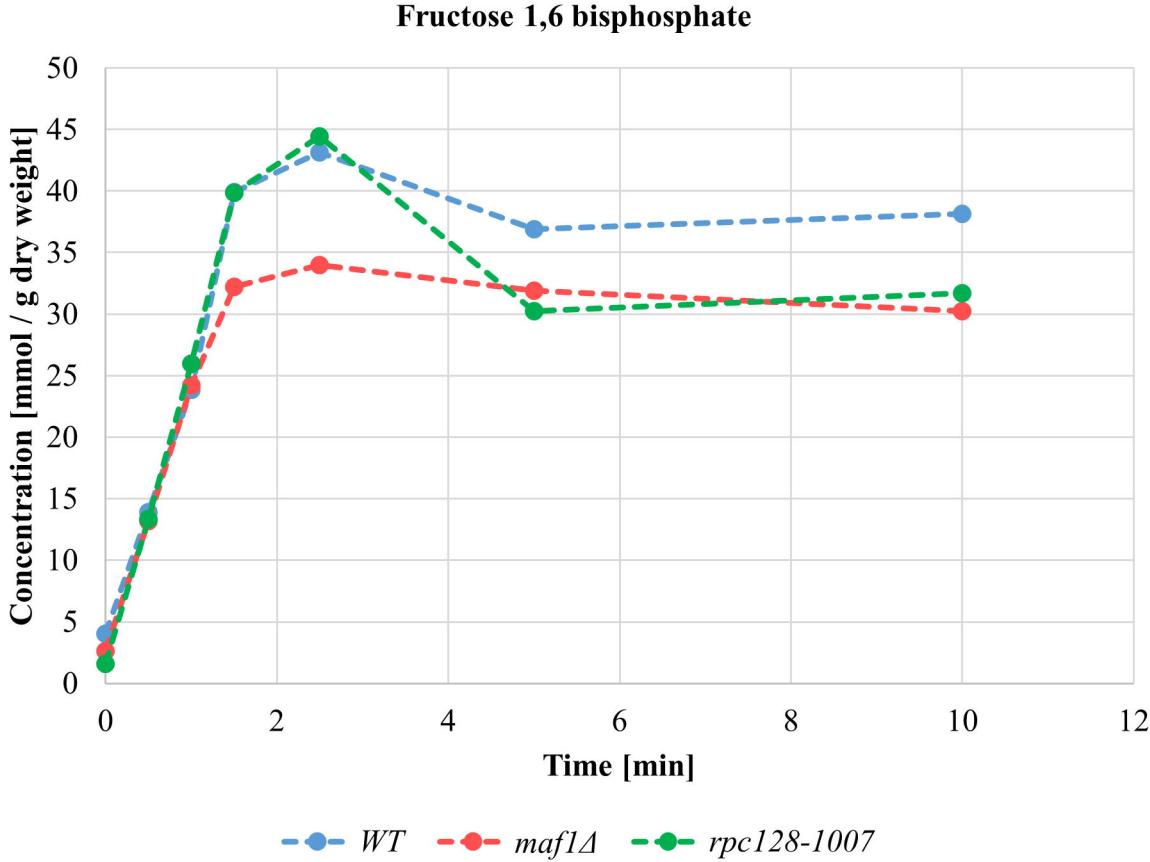
Fructose 1,6 bisphosphate
Concentration [mmol / g dry weight]
50
45
40
35
30
25
20
15
10
5
0
0
2
4
6
8
10
12
Time [min]
WT
maf1Δ
rpc128-1007

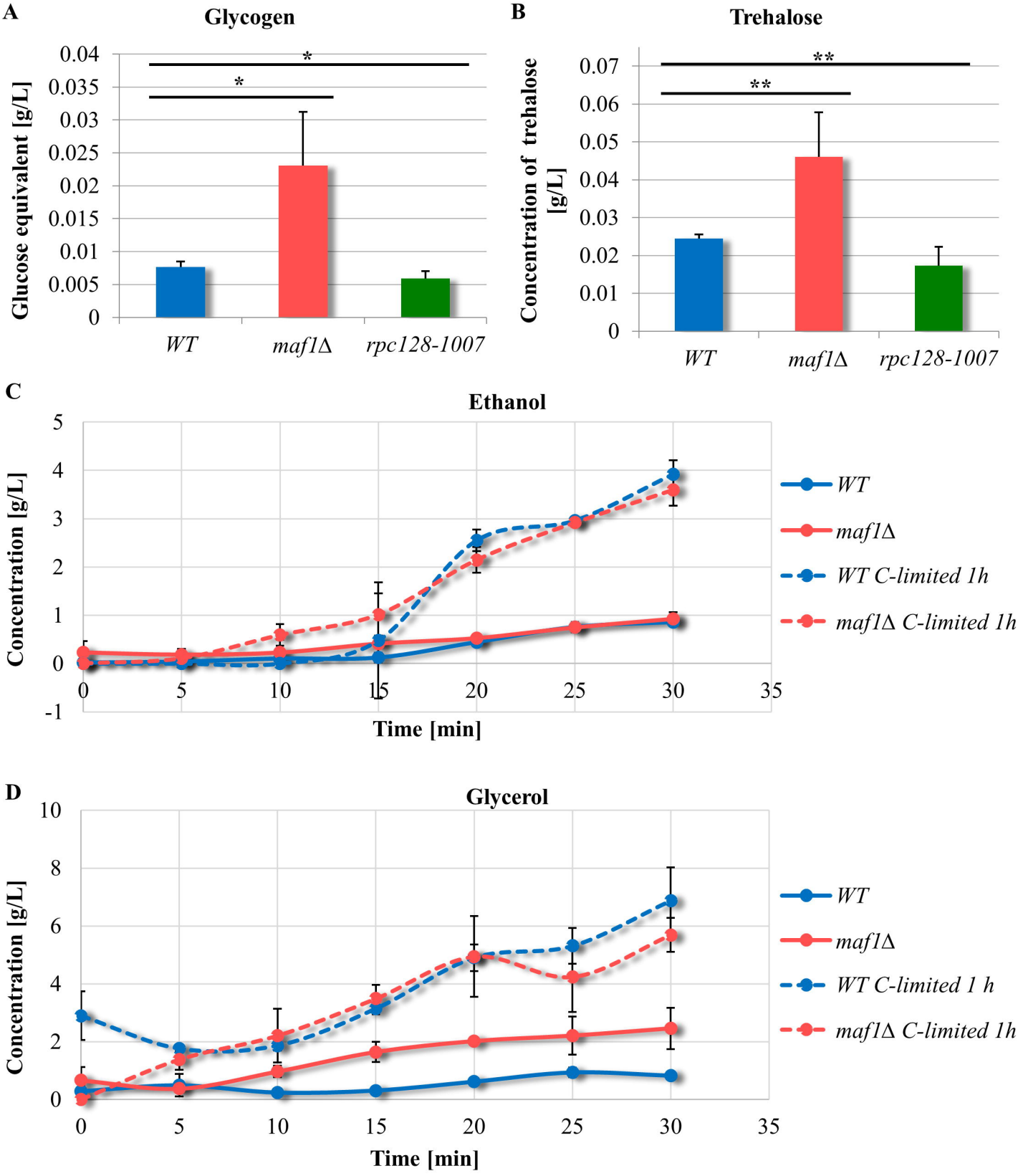
A
Glycogen
Glucose equivalent [g/L]
0.04
0.035
0.03
0.025
0.02
0.015
0.01
0.005
0
*
*
WT
maf1Δ
rpc128-1007
B
Trehalose
Concentration of trehalose [g/L]
0.07
0.06
0.05
0.04
0.03
0.02
0.01
0
**
**
WT
maf1Δ
rpc128-1007
C
Ethanol
Concentration [g/L]
5
4
3
2
1
0
-1
0
5
10
15
20
25
30
35
Time [min]
WT
maf1Δ
WT C-limited 1h
maf1Δ C-limited 1h
D
Glycerol
Concentration [g/L]
10
8
6
4
2
0
0
5
10
15
20
25
30
35
Time [min]
WT
maf1Δ
WT C-limited 1 h
maf1Δ C-limited 1h

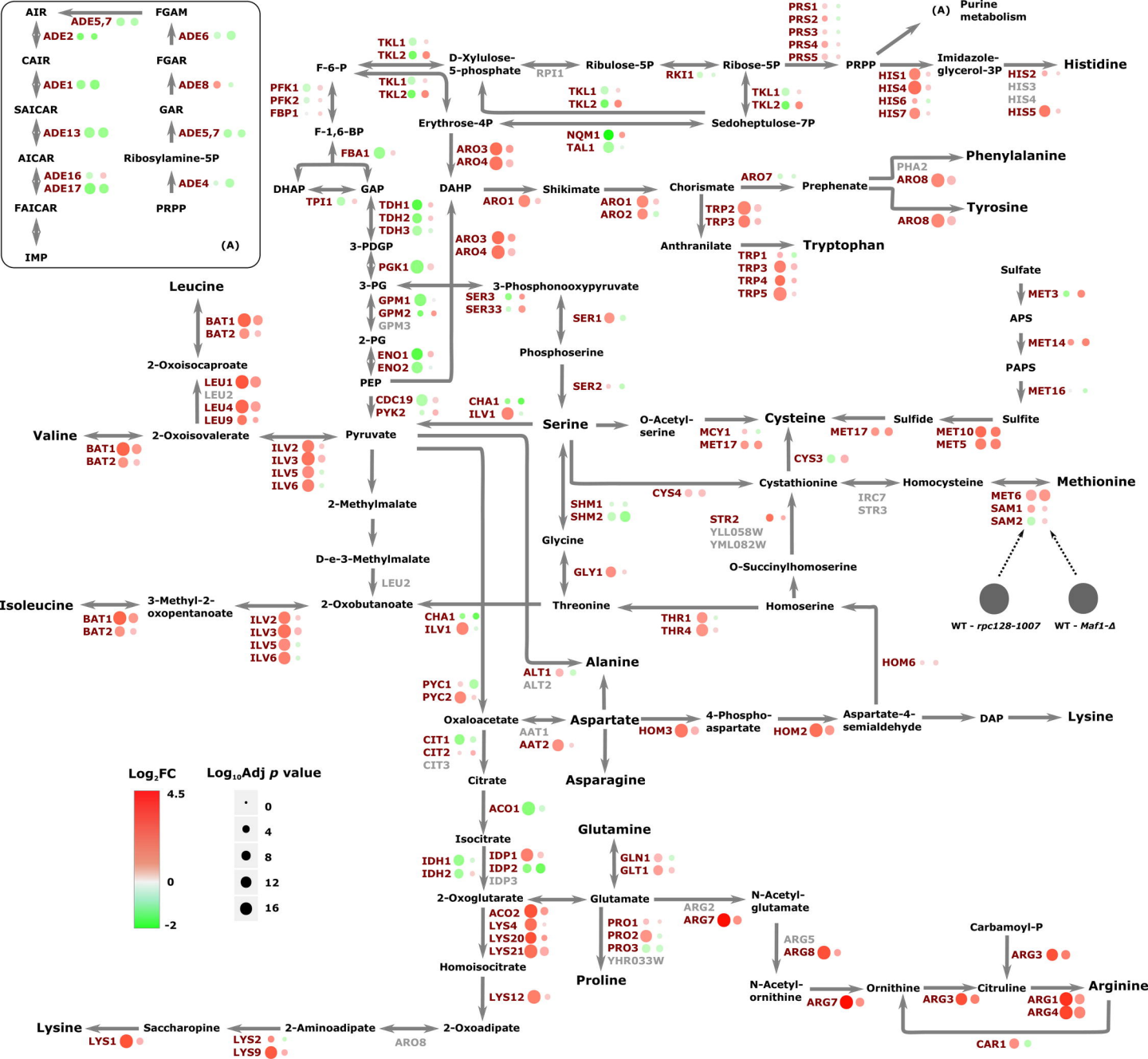
AIR
ADE5,7
FGAM
ADE2
ADE6
CAIR
FGAR
ADE1
ADE8
SAICAR
GAR
ADE13
ADE5,7
AICAR
Ribosylamine-5P
ADE16
ADE17
ADE4
FAICAR
PRPP
IMP
(A)
(A) Purine metabolism
PRS1
PRS2
PRS3
PRS4
PRS5
PRPP
Imidazole-glycerol-3P
HIS1
HIS4
HIS6
HIS7
HIS2
HIS3
HIS4
HIS5
Histidine
TKL1
TKL2
F-6-P
D-Xylulose-5-phosphate
RPI1
Ribulose-5P
RKI1
Ribose-5P
PFK1
PFK2
FBP1
F-1,6-BP
Erythrose-4P
Sedoheptulose-7P
NQM1
TAL1
FBA1
ARO3
ARO4
DHAP
GAP
DAHP
ARO1
Shikimate
Chorismate
ARO7
Prephenate
PHA2
ARO8
Phenylalanine
Tyrosine
TPI1
TDH1
TDH2
TDH3
ARO1
ARO2
TRP2
TRP3
Anthranilate
Tryptophan
3-PDGP
PGK1
3-PG
3-Phosphonooxypyruvate
SER3
SER33
SER1
GPM1
GPM2
GPM3
2-PG
ENO1
ENO2
PEP
Phosphoserine
SER2
TRP1
TRP3
TRP4
TRP5
Sulfate
MET3
APS
MET14
PAPS
MET16
Leucine
BAT1
BAT2
2-Oxoisocaproate
LEU1
LEU2
LEU4
LEU9
CDC19
PYK2
CHA1
ILV1
Serine
O-Acetyl-serine
MCY1
MET17
Cysteine
MET17
Sulfide
Sulfite
MET10
MET5
CYS3
Valine
2-Oxoisovalerate
Pyruvate
ILV2
ILV3
ILV5
ILV6
CYS4
Cystathionine
IRC7
STR3
Homocysteine
Methionine
MET6
SAM1
SAM2
2-Methylmalate
SHM1
SHM2
STR2
YLL058W
YML082W
Glycine
O-Succinylhomoserine
D-e-3-Methylmalate
LEU2
GLY1
Isoleucine
3-Methyl-2-oxopentanoate
2-Oxobutanoate
Threonine
Homoserine
THR1
THR4
WT - rpc128-1007
WT - Maf1-Δ
Alanine
ALT1
ALT2
HOM6
PYC1
PYC2
Oxaloacetate
Aspartate
HOM3
4-Phospho-aspartate
HOM2
Aspartate-4-semialdehyde
DAP
Lysine
AAT1
AAT2
CIT1
CIT2
CIT3
Citrate
Asparagine
Log2FC
4.5
0
-2
Log10Adj p value
0
4
8
12
16
ACO1
Isocitrate
Glutamine
IDH1
IDH2
IDP1
IDP2
IDP3
GLN1
GLT1
2-Oxoglutarate
Glutamate
N-Acetyl-glutamate
ARG2
ARG7
ACO2
LYS4
LYS20
LYS21
PRO1
PRO2
PRO3
YHR033W
ARG5
ARG8
Carbamoyl-P
ARG3
Homoisocitrate
Proline
N-Acetyl-ornithine
ARG7
Ornithine
ARG3
Citruline
ARG1
ARG4
Arginine
LYS12
CAR1
Lysine
LYS1
Saccharopine
LYS2
LYS9
2-Aminoadipate
ARO8
2-Oxoadipate

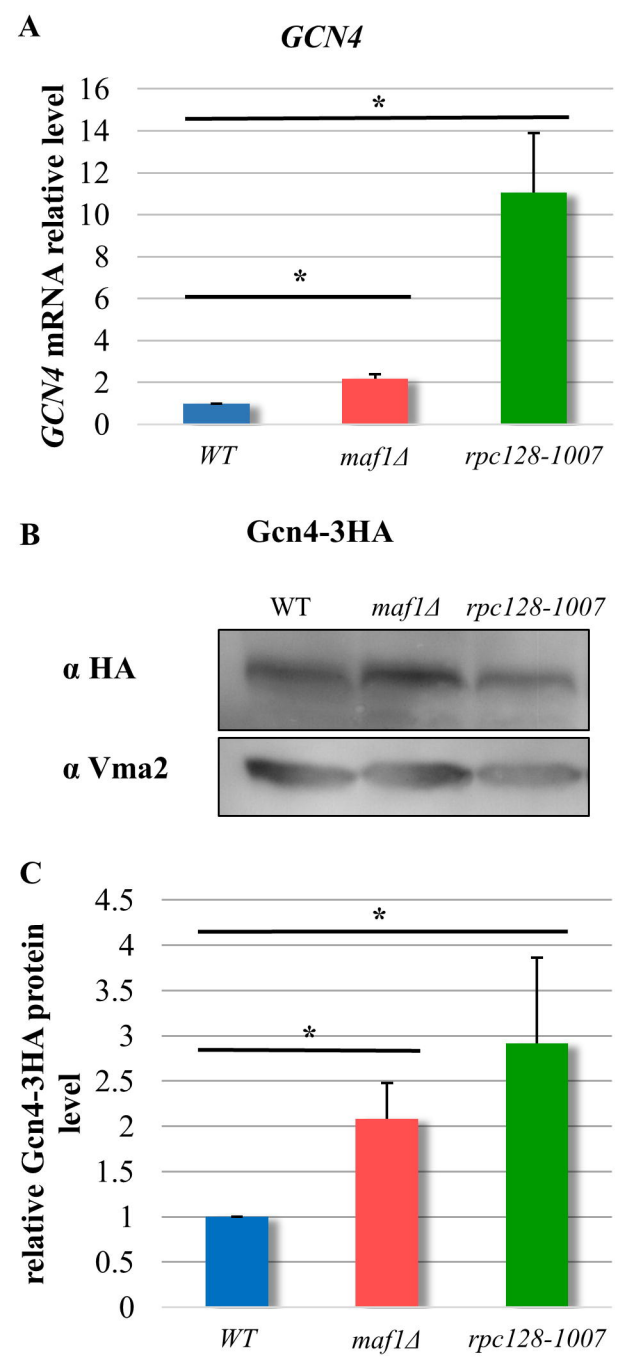
A
GCN4
GCN4 mRNA relative level
16
14
12
10
8
6
4
2
0
*
*
WT
maf1Δ
rpc128-1007
B
Gcn4-3HA
WT
maf1Δ
rpc128-1007
α HA
α Vma2
C
relative Gcn4-3HA protein level
4.5
4
3.5
3
2.5
2
1.5
1
0.5
0
*
*
WT
maf1Δ
rpc128-1007

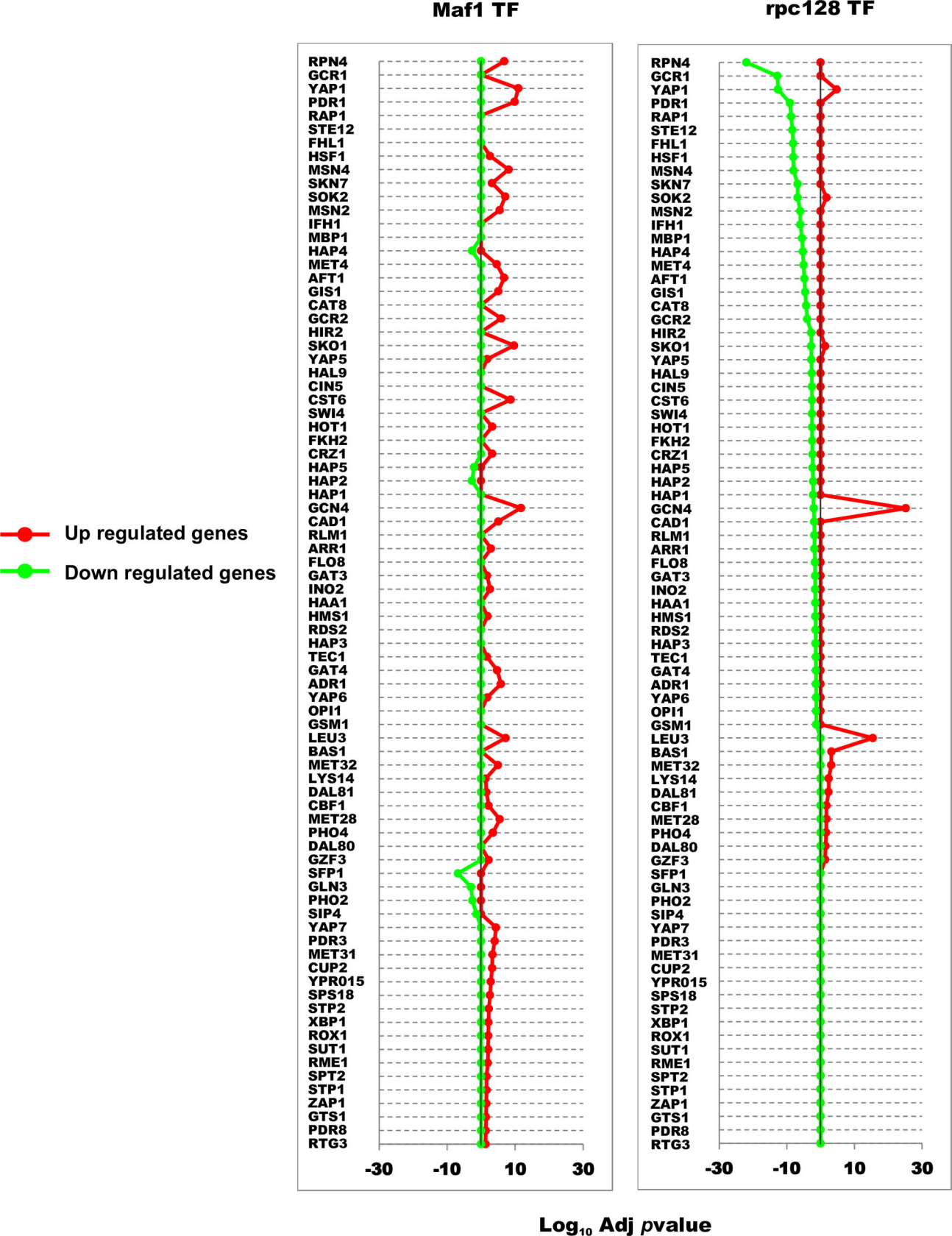
Maf1 TF
rpc128 TF
Up regulated genes
Down regulated genes
RPN4
GCR1
YAP1
PDR1
RAP1
STE12
FHL1
HSF1
MSN4
SKN7
SOK2
MSN2
IFH1
MBP1
HAP4
MET4
AFT1
GIS1
CAT8
GCR2
HIR2
SKO1
YAP5
HAL9
CIN5
CST6
SWI4
HOT1
FKH2
CRZ1
HAP5
HAP2
HAP1
GCN4
CAD1
RLM1
ARR1
FLO8
GAT3
INO2
HAA1
HMS1
RDS2
HAP3
TEC1
GAT4
ADR1
YAP6
OPI1
GSM1
LEU3
BAS1
MET32
LYS14
DAL81
CBF1
MET28
PHO4
DAL80
GZF3
SFP1
GLN3
PHO2
SIP4
YAP7
PDR3
MET31
CUP2
YPR015
SPS18
STP2
XBP1
ROX1
SUT1
RME1
SPT2
STP1
ZAP1
GTS1
PDR8
RTG3
-30
-10
10
30
Log10 Adj pvalue

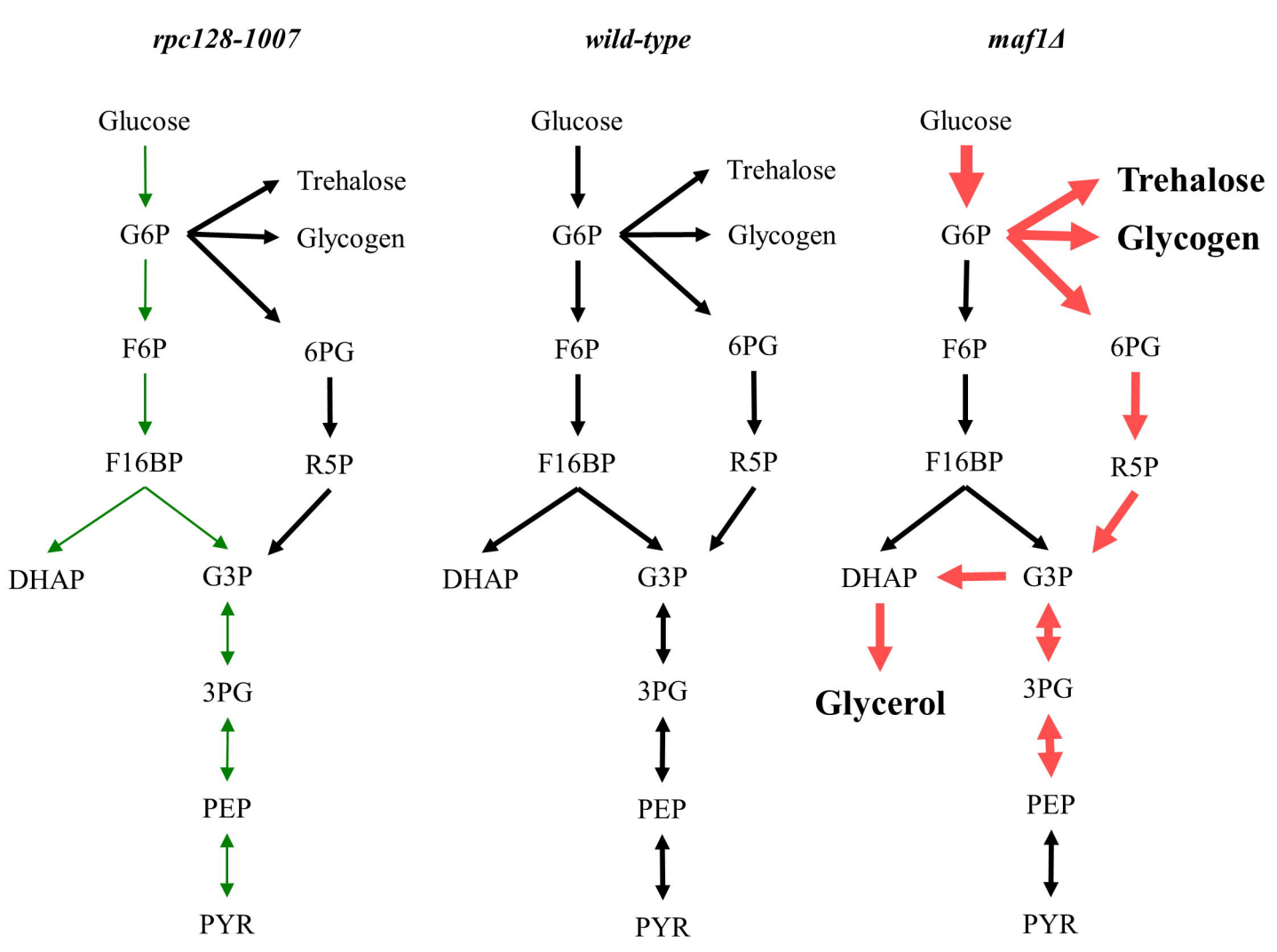
rpc128-1007
wild-type
maf1Δ
Glucose
Trehalose
G6P
Glycogen
F6P
6PG
F16BP
R5P
DHAP
G3P
3PG
PEP
PYR
Glucose
Trehalose
G6P
Glycogen
F6P
6PG
F16BP
R5P
DHAP
G3P
3PG
PEP
PYR
Glucose
Trehalose
G6P
Glycogen
F6P
6PG
F16BP
R5P
DHAP
G3P
Glycerol
3PG
PEP
PYR